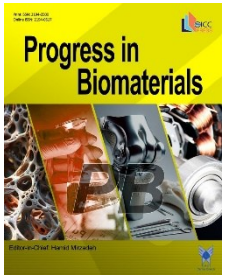

Volume 14, Issue 2, 2025: Article 6

Progress in Biomaterials (PIBM)

https://doi.org/10.57647/pibm.2025.1402.33

Preparation and Evaluation of Physical and Biological Properties of Three-Dimensional Scaffolds Based on Poly (glycerol succinic acid) (PGSU) and Chitosan for Use in Soft Tissue Engineering

Faezesadat Miri[1], Soheila Zamanlui benisi[1], Samira Farjaminejad [2], Mohammad Hossein Allahyari [1], Nadia Rezavand [3], Shahrokh Shojaei [1], Pedram Tehrani [1], Milad Jafari-Nodoushan [1], Wei-Hsin Chen [4,5,6] , Vahabodin Goodarzi[7,*]

[1] *Department of Biomedical Engineering, CT.C., Islamic Azad University, Tehran, Iran*
[2] *School of Health and Psychological Sciences, Department of Health Services Research and Management, University of London, London WC1E 7HU, U.K*
[3] *Institute of Biomaterials, University of Tehran & Tehran University of Medical Science (IBUTMS), Tehran, Iran*
[4] *Department of Mechanical Engineering, National Chin-Yi University of Technology, Taichung, 411, Taiwan*
[5] *Department of Aeronautics and Astronautics, National Cheng Kung University, Tainan, 701, Taiwan*
[6] *Research Center for Smart Sustainable Circular Economy, Tunghai University, Taichung, 407, Taiwan*
[7] *Tissue Engineering and Regenerative Medicine Research Center, Baqiyatallah University of Medical Sciences, Tehran, Iran*

***Corresponding author:** v.goodarzi@hotmail.com

Original Research

Received:
04 March 2025

Accepted:
09 May 2025

Published in Issue:
30 June 2025

Abstract

The development of biocompatible, biodegradable, and structurally adaptable scaffolds remains a critical challenge in tissue engineering. In this study, a series of novel three-dimensional porous scaffolds were fabricated by combining poly (glycerol succinate) (PGSu) with varying weight ratios of chitosan (Ch) using a salt-leaching technique. The chemical structure and functional group interactions were confirmed through Fourier-transform infrared spectroscopy (FTIR) analysis. X-ray diffraction (XRD) revealed enhanced molecular ordering in Cs-rich compositions. Scanning electron microscopy (SEM) demonstrate that the incorporation of Cs improved pore interconnectivity and surface roughness. Contact angle measurements and swelling tests indicated increased hydrophilicity and water uptake, particularly in PGSu/Cs (30/70) scaffolds. Mechanical testing revealed that PGSu/Ch (50/50) exhibited superior compressive strength and elasticity under both dry and hydrated conditions, while PGSu/Ch (30/70) demonstrated enhanced flexibility and deformability in wet environments which is an essential feature for tissue applications. Thermogravimetric analysis (TGA) and hydrolytic degradation in fetal bovine serum (FBS) revealed that Ch content modulated scaffold thermal stability and biodegradation rate, with PGSu/Ch (30/70) degrading most rapidly over 60 days. Biological assessments, including MTT assay and SEM-based cell adhesion analysis, confirmed excellent

cytocompatibility for all PGSu/Ch scaffolds. The PGSu/Ch (30/70) composition demonstrated the highest levels of cell viability, adhesion, and surface colonization over a 7-day culture period. These findings highlight the potential of PGSu/Ch scaffolds as tunable biomaterials for soft tissue regeneration, offering a favorable balance between mechanical performance, biodegradability, and cellular compatibility.

Keywords: Poly (glycerol succinate) (PGSu), Chitosan-based scaffold, Porous biomaterial, Tissue engineering

Cite this article: Miri F., Zamanlui benisi S., Farjaminejad S., Allahyari M.H., Rezavand N., Shojaei Sh., Tehrani P., Jafari-Nodoushan M., Chen W.H., Goodarzig V., Preparation and Evaluation of Physical and Biological Properties of Three-Dimensional Scaffolds Based on Poly (glycerol succinic acid) (PGSU) and Chitosan for Use in Soft Tissue Engineering. *Progress in Biomaterials,* 14(2), Article 6. https://doi.org/10.57647/pibm.2025.1402.33

Graphical in Biomaterials

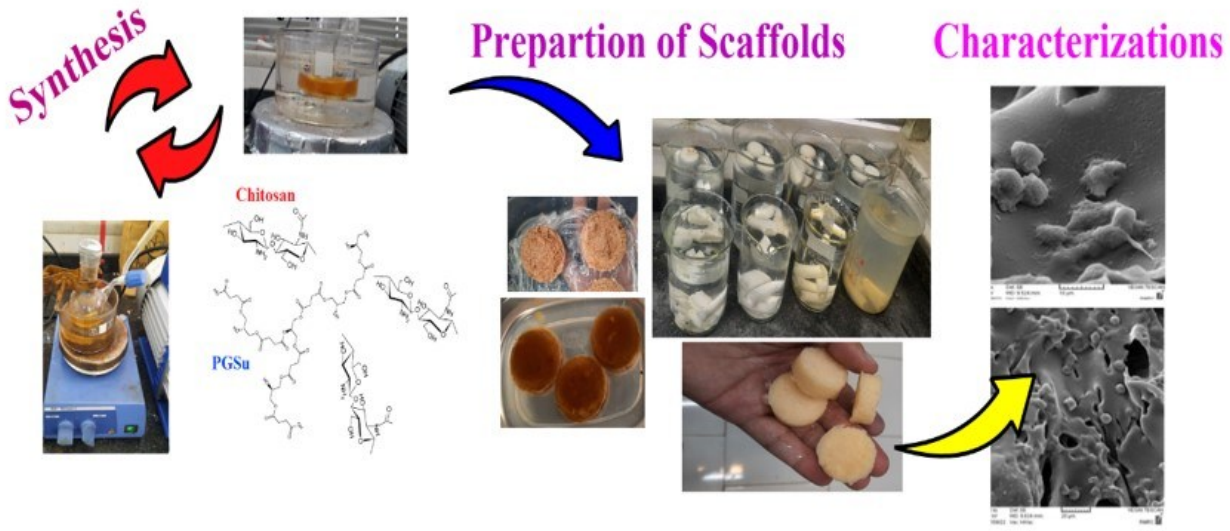

1. Introduction

Tissue engineering has emerged as a leading interdisciplinary field in regenerative medicine, offering innovative strategies for restoring or replacing damaged tissues and organs by combining biomaterials, cells, and signaling molecules [1][2][3][4]. At the heart of tissue engineering lies the design of three-dimensional scaffolds that mimic the architecture and function of the extracellular matrix (ECM), offering not only structural support but also essential biochemical cues to facilitate cell adhesion, proliferation, and lineage-specific differentiation [5]. The selection and engineering of scaffold materials with optimized physicochemical and biological properties are critical to the success of tissue regeneration strategies [6].

Biodegradable polyesters synthesized via condensation reactions between polyfunctional alcohols and carboxylic acids have shown considerable promise in scaffold fabrication due to their tunable degradation profiles, mechanical properties, and cytocompatibility[7]. Among these, poly (glycerol sebacate) (PGS), synthesized from glycerol and sebacic acid, has been extensively studied for its elastomeric behavior and suitability in both soft and hard tissue engineering applications [8]. Nonetheless, the need for materials with improved hydrophilicity, degradation rates, and crosslinking potential has prompted the exploration of alternative monomers. Succinic acid, a naturally derived, biocompatible dicarboxylic acid, has attracted interest in this context due to its short aliphatic chain and high polarity[9].

Poly (glycerol succinic acid) (PGSu), obtained from the polycondensation of glycerol and succinic acid, possesses a higher density of ester linkages and fewer hydrophobic segments than PGS, potentially enhancing its hydrolytic degradability and functional versatility. Despite these advantages, PGSu remains relatively

underexplored in the literature[10]. Zabihi et al. synthesized PGSu-based nanogels in a single-step method and demonstrated their efficacy for dermal delivery applications [11]. Similarly, Luman and co-workers developed dendritic macromolecules from glycerol, succinic acid, and polyethylene glycol (PEG), showcasing their biomedical potential [12]. Additional studies have shown that succinic acid-based co-polymers exhibit tunable mechanical, thermal, and biological properties when combined with other monomers such as sebacic acid or ε-caprolactone [13][14].

Recent investigations have also explored the blending of PGSu with other biodegradable polymers to enhance its structural and functional attributes. Mahtabi et al. developed a three-dimensional composite scaffold composed of polylactic acid (PLA), PGSu, and nano-hydroxyapatite, demonstrating its potential for bone tissue engineering applications due to improved mechanical integrity and biocompatibility [15]. In another study, PGSu was incorporated into polycaprolactone-based nanocomposites, resulting in enhanced mechanical strength, flexibility, and scaffold interconnectivity, all of which are desirable properties for soft tissue regeneration [16].

The integration of natural polymers with synthetic scaffolds has been shown to improve biological performance by promoting better biocompatibility, cell adhesion, and tissue integration. Chitosan (Ch), a polysaccharide derived from chitin, has attracted widespread attention due to its biodegradability, non-toxicity, antibacterial activity, and ability to support cellular adhesion and proliferation[17]. The combination of chitosan with synthetic polyesters such as PGS has been shown to enhance scaffold hydrophilicity, degradation behavior, and cell–material interactions[18]. For instance, Zhang et al. demonstrated improved cellular affinity in scaffolds composed of PGS, silk fibroin, and Ch for skin tissue engineering [19]. Other studies have employed modified poly (glycerol sebacate citric)/Ch/hydroxyapatite nanocomposites [20], as well as Ch–gelatin–PGS blends [21], all of which have shown promise for various tissue engineering applications. Furthermore, Rostamian et al. introduced a biodegradable nanocomposite scaffold based on Ch, PGS, and graphene oxide, revealing its potential for biomedical and environmental applications [22].

Despite these advancements, the combination of PGSu and Ch has not been thoroughly investigated, particularly in the context of porous 3D scaffolds designed for soft tissue regeneration. The integration of PGSu with Ch may offer synergistic advantages: PGSu provides structural flexibility and tunable degradation[23], while Ch contributes biological activity and enhances cell affinity[24]. The interaction between the ester and amine/hydroxyl groups of these two polymers could enable improved crosslinking, mechanical resilience, and biocompatibility[25].

This study aims to develop and characterize three-dimensional porous scaffolds composed of PGSu and Ch using the salt-leaching technique. By systematically varying the Ch content, we investigated its impact on scaffold architecture, mechanical behavior, hydrolytic degradation, and *in vitro* cellular responses. The rationale for combining PGSu with chitosan lies in their complementary chemical structures, which enable hydrogen bonding, enhance crosslinking, and improve biological interactions, thereby offering a promising material platform for soft tissue engineering. Furthermore, the salt-leaching method provides a simple, scalable, and cost-effective fabrication route to achieve scaffolds with controlled porosity and interconnected networks, which are essential for nutrient transport, cell infiltration, and tissue vascularization. The insights obtained from this work may contribute to the rational design of adaptable, biofunctional scaffolds for applications in skin, muscle, and peripheral nerve regeneration, where structural integrity, biodegradability, and biocompatibility must be finely balanced [26].

This work represents the first systematic investigation of PGSu/Ch composite scaffolds across multiple weight ratios, establishing direct correlations between Ch content, mechanical performance, hydrolytic degradation kinetics, and cell–material interactions. In contrast to the work of Zabihi et al. on PGSu-based nanogels [11] and Mahtabi et al. on PLA/PGSu/nHA bone scaffolds [15], our investigation is focused on soft tissue engineering and uniquely elucidates how compositional tuning governs structural adaptability and viscoelastic behavior under hydrated conditions. This integrated approach addresses a critical knowledge gap by linking physicochemical properties to biological functionality, thereby providing a rational design framework for PGSu/Ch scaffolds tailored to specific regenerative applications.

2. Experimental

2.1. Materials

All chemicals used in this study were of analytical grade and procured from reputable suppliers. Glycerol, succinic acid, and chitosan (medium molecular weight) were obtained from Sigma-Aldrich (USA). Sodium chloride (NaCl, particle size <200 µm), N, N-dimethylformamide (DMF), and hexamethylene

diisocyanate (HDI) were purchased from Merck (Germany). Tin (II) 2-ethylhexanoate (tin octanoate) was also supplied by Sigma-Aldrich and used as a catalyst without further purification.

2.2. Preparation of scaffolds

In the first step, PGSu resin was synthesized via a direct polycondensation reaction. Equimolar amounts of glycerol and succinic acid were accurately measured and transferred into a reaction vessel. The mixture was heated to 160 °C under constant stirring for 3 hours to initiate esterification. Subsequently, a vacuum was applied to the system and maintained for an additional 4 hours to promote further polycondensation and remove water byproducts. After completion, the reaction was terminated by ceasing the heat supply, and the resulting PGSu resin was collected and stored for subsequent use.

To fabricate the final scaffold formulations, the obtained PGSu resin was dissolved in a solvent mixture of dioxane and dimethyl sulfoxide (DMSO) at a volume ratio of 30:70. The solution was stirred at room temperature for 12 hours to ensure complete dissolution. Ch was then incorporated at varying weight ratios (30, 50, and 70 wt.%), and the mixture was stirred until a homogenous polymeric solution was achieved. Tin (II) 2-ethylhexanoate (tin octanoate) was added as a catalyst, and the reaction was maintained at 50 °C with continued stirring for 30 minutes. Subsequently, hexamethylene diisocyanate (HDI) was introduced as a chemical crosslinking agent, and the mixture was stirred for an additional 10 minutes until a noticeable increase in viscosity was observed. To ensure reproducibility of synthesized PGSu, the polycondensation reaction was performed under strictly controlled temperature and vacuum conditions, and the viscosity of each batch was monitored to confirm consistent molecular weight range across preparations. Although molecular weight determination by GPC was not included in this study, the reproducibility of mechanical and degradation profiles across independent batches confirmed consistent polymer properties. The solvent system consisting of dioxane/DMSO (30:70 v/v) was selected based on preliminary solubility tests to provide optimal dissolution of PGSu and chitosan while maintaining a homogeneous solution with manageable viscosity, which is critical for achieving uniform pore distribution during salt-leaching. After casting, the scaffolds were dried under ambient conditions for two weeks followed by an additional vacuum-drying step to ensure complete solvent removal, thereby minimizing any potential cytotoxicity from residual solvent. To mitigate any cytotoxic effects of unreacted HDI, the crosslinked scaffolds were subjected to extensive washing with deionized water for 72 h with multiple water exchanges, followed by secondary drying under vacuum. This process was verified to remove unreacted HDI and its byproducts, ensuring biocompatibility prior to further characterization and biological testing. Sodium chloride (NaCl) particles (particle size <200 µm) were then added as porogens. The final mixture was poured into pre-prepared cylindrical molds (3 cm in diameter) and allowed to dry at ambient temperature for two weeks to enable solidification and solvent evaporation. Following the drying period, the scaffolds were immersed in distilled water to leach out the salt particles and create a porous structure. The samples were then dried again for one week under ambient conditions and stored for further characterization and testing. The composition and coding of the fabricated samples are summarized in Table 1. An overview of the fabrication process and representative scaffold morphology is presented in Scheme 1.

Table 1. Sample codes and composition of prepared samples

Sample	PGSu (wt.%)	Ch (wt.%)
PGSu	100	-
PGSu70/Ch30	70	30
PGSu30/Ch70	30	70
PGSu50/Ch50	50	50

Alternative approaches could have been employed for both synthesis and scaffold fabrication. For instance, PGSu could be synthesized via enzymatic polycondensation or solution-mediated step-growth reactions, and scaffold fabrication could have been performed using electrospinning, lyophilization, or 3D printing to generate fibrous or gradient architectures. Likewise, micro-CT or mercury intrusion porosimetry could have been used to determine pore size distribution more precisely, and tensile or cyclic loading tests could complement the mechanical analysis.

In this work, direct melt polycondensation was selected to avoid the use of toxic catalysts or solvents, ensuring a reproducible, cost-effective, and environmentally benign route. The salt-leaching technique was chosen for its simplicity, scalability, and ability to create interconnected macroporous networks that are critical for nutrient transport, cell infiltration, and neovascularization in soft tissue regeneration. Compression testing under dry and hydrated conditions was prioritized because it reflects the physiologically dominant loading mode for dermal, subcutaneous, and peripheral nerve tissues. These choices collectively ensured clinically relevant scaffold properties while maintaining biocompatibility and experimental reproducibility.

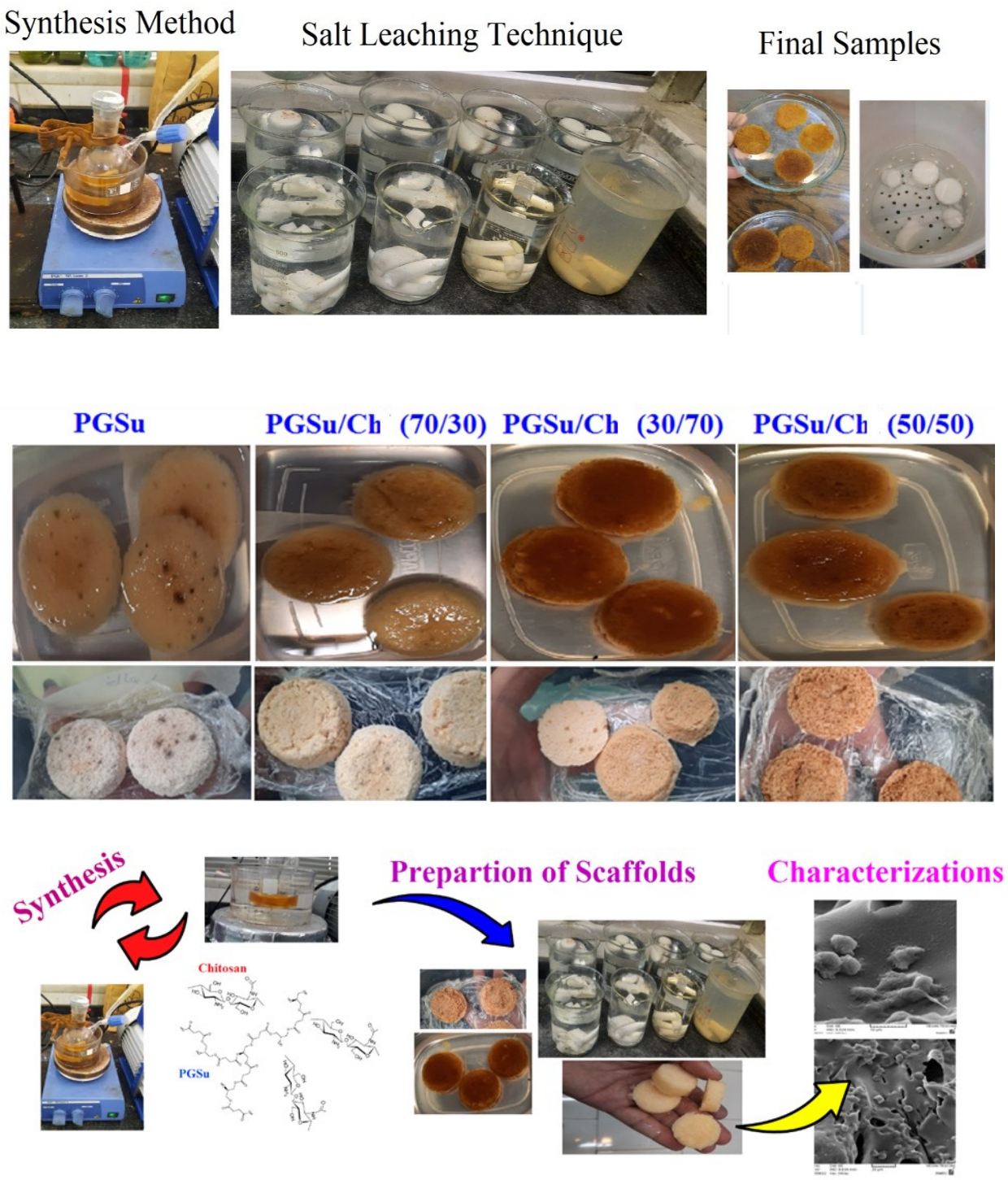

Scheme 1. Images of the process of preparing 3D scaffolds using the salt leaching technique

2.3. Characterizations

Fourier transform infrared spectroscopy (FTIR) was conducted using a Thermo Nicolet Nexus 470 FTIR instrument (USA) equipped with an attenuated total reflectance (ATR) module. ATR-FTIR was employed to identify the functional groups in the pure components and to assess chemical interactions within the fabricated PGSu/chitosan scaffolds. The surface morphology and internal microstructure of the scaffolds were examined by scanning electron microscopy (SEM, Philips, Netherlands). Prior to imaging, the samples were sputter-coated with a thin layer of gold and platinum for 20 minutes to enhance conductivity. SEM images were captured at various magnifications to evaluate pore architecture and surface topology, and quantitative image analysis was subsequently performed using ImageJ (NIH, Bethesda, MD, USA) to determine surface

porosity and pore size distribution. Thermal stability and degradation behavior of the scaffolds were analyzed using thermogravimetric analysis (TGA, Model Q1000, TA Instruments, USA). Approximately 10 mg of each sample was heated from room temperature to 700 °C at a constant heating rate of 10 °C/min under a nitrogen atmosphere. Crystallinity and phase structure of the scaffolds were evaluated via X-ray diffraction (XRD) using an AWXD M300 diffractometer with Cu Kα radiation (λ = 1.5406 Å), scanned over a 2θ range of 10°–35°. Wettability and surface hydrophilicity of the scaffolds were assessed through dynamic water contact angle measurements. A water droplet was placed on the scaffold surface, and images were recorded every 15 seconds for 60 seconds. The left and right contact angles were measured and averaged to determine hydrophilicity over time. Mechanical properties of the scaffolds under compressive loading were measured using a universal testing machine (Zwick/Roell Z050, Germany) equipped with a 10 N load cell. Cylindrical specimens (2 cm diameter × 5 cm height) were compressed at a strain rate of 1 mm/min. Compressive modulus and ultimate strength were calculated from the initial linear (elastic) region and maximum point on the stress–strain curve, respectively. PGSu/Ch scaffolds were incubated in phosphate-buffered saline (PBS, pH 7.4) supplemented with 10% fetal bovine serum (FBS) at 37 °C under gentle shaking for up to 28 days. No enzymes or other catalytic agents were added; thus, mass loss is attributed solely to hydrolysis of the polyester network in a physiologically relevant aqueous environment. Scaffolds were removed at predetermined intervals (7, 14, 21, and 28 days), gently rinsed with deionized water to remove salts, lyophilized, and weighed to determine percentage mass loss. Cell viability was evaluated using the MTT assay. Cells were seeded on sterilized scaffolds and incubated for 1, 3, and 5 days (24, 72, and 120 hours). At each time point, the culture medium was replaced with 200 µL of MTT solution (0.5 mg/mL, Sigma-Aldrich) and incubated for 4 hours to allow formation of formazan crystals. Subsequently, 200 µL of DMSO was added to solubilize the crystals, and the absorbance was measured at 570 nm using a microplate reader (Expert 96, Asys Hitch, Austria). Experiments were conducted in triplicate (n = 3). Cell adhesion and morphology were further evaluated by SEM after 5 days of culture. The scaffolds were fixed with 2% paraformaldehyde and 2.5% glutaraldehyde for 90 minutes at room temperature. Samples were rinsed twice with phosphate-buffered saline (PBS), then dehydrated through a graded ethanol series (30%, 50%, 70%, 85%, 90%, and 100%, 5 minutes each). The samples were then dried and sputter-coated with gold prior to SEM imaging. To determine the cell viability, Equation (1) is used. In this equation, OD_e, OD_c, and OD_b correspond respectively to the absorption peak intensity at 570 nanometers for cell-containing scaffolds, control samples, and empty plates[2].

$$Cell\ viability\ (\%) = \frac{(OD_e - OD_b)}{(OD_c - OD_b)} \times 100 \quad (1)$$

All quantitative data are presented as mean ± standard deviation (SD). Statistical analysis was performed using one-way analysis of variance (ANOVA), followed by Tukey's post hoc test. A p-value less than 0.05 was considered statistically significant.

3. Results and discussion

3.1. FTIR analysis

Figure 1A presents the ATR-FTIR spectra of glycerol, succinic acid, and PGSu. PGSu displays a new and strong peak near 1730 cm^{-1}, corresponding to the stretching vibration of ester carbonyl groups, which is absent in the monomer spectra [27][28]. This confirms the formation of ester bonds[29]. Additionally, the broad band at 3400 cm^{-1}, attributed to OH stretching, indicates the presence of residual hydroxyl groups in the polymer structure[30]. Figure 1B compares the FTIR spectra of PGSu and Ch. Both materials exhibit broad bands around 3400 cm^{-1} due to –OH and $–NH_2$ groups[31], while PGSu retains its ester peak at 1730 cm^{-1}. The overlap of functional groups suggests potential for hydrogen bonding and chemical crosslinking when PGSu and Ch are combined, which is critical for scaffold stability and performance[32]. The chemical interactions within the PGSu/Ch composite scaffolds are illustrated in Figure 1C. As the Ch content increases from 30 wt% to 70 wt%, the intensity and breadth of the OH/NH_2 stretching band at 3400 cm^{-1} significantly increase. This reflects the incorporation of more polar groups from Ch, enhancing the scaffold's hydrophilicity and potential reactivity[33]. In the PGSu/Cs 70/30 formulation, the increase in intensity is modest, suggesting partial integration of Ch. In contrast, the PGSu/Ch 30/70 scaffold exhibits a highly broadened and intense peak at 3400 cm^{-1}, indicating a saturated presence of hydroxyl and amine groups from Ch. This suggests strong interpolymer interactions and greater potential for crosslinking and water absorption[34]. The PGSu/Cs (50/50) sample exhibited FTIR peaks characteristic of both constituents, including a moderately intense broad band around 3400 cm^{-1} (–OH and $–NH_2$ stretching) and a sharp ester C=O peak near 1700 cm^{-1}. The intermediate intensity and lack of significant peak shift suggest balanced intermolecular interactions and a stable

chemical environment within the scaffold matrix. Notably, in all scaffold compositions, the ester carbonyl peak at 1730 cm^{-1} remains prominent and stable, indicating that the backbone structure of PGSu is preserved during blending and scaffold fabrication.

3.2. Microstructure analysis

The microstructure of the fabricated scaffolds was investigated using SEM, and representative images at various magnifications, along with macro-scale appearances, are shown in Figure 2.

The pure PGSu scaffold (Figures 2A and 2A′) exhibits a relatively dense structure with a limited number of open and interconnected pores. This morphology can be attributed to the high degree of crosslinking among PGSu chains, where most of the hydroxyl and carboxyl groups are involved in the formation of ester bonds, leaving fewer functional sites to facilitate pore formation[35]. At lower magnification (Figure 2A), the scaffold surface displays moderate roughness, which could aid initial cell attachment. However, the overall porosity appears suboptimal for applications requiring enhanced cellular infiltration and nutrient transport. The incorporation of 30 wt% Ch into the PGSu matrix (PGSu/Ch 70/30; Figures 2B and 2B′) leads to an increase in the number and interconnectivity of pores. The structure exhibits thinner pore walls and a more open morphology compared to pure PGSu. This improvement is likely due to the hydrophilic nature and rich functional groups of Ch, which influence phase separation and facilitate the development of porous networks during fabrication[36]. The macrostructure (Figure 2B″) also confirms a more uniform porous distribution, though still with some density retained. The PGSu/Ch (50/50) scaffold (Figure 2C and 2C′) demonstrates a well-organized and highly interconnected porous network with uniformly distributed pores ranging approximately from 11 to 25 µm. The balanced composition between PGSu and Ch creates an optimal environment for phase separation, leading to stable pore formation and well-structured pore walls[37]. This morphology is particularly favorable for cell infiltration and nutrient diffusion. Furthermore, the coexistence of ester (PGSu) and amine/hydroxyl (Ch) functional groups, as previously confirmed by FTIR analysis (Figure 1E), may enhance scaffold stability through hydrogen bonding and chemical crosslinking. The macrostructure (Figure 2C″) supports this observation, showing a uniformly porous surface indicative of a well-developed 3D architecture. In the PGSu/Cs (30/70) scaffold (Figures 2D and 2D′), a highly porous, sponge-like morphology is observed, characterized by thinner pore walls and a more irregular but interconnected structure. The high concentration of Ch, with its hydrophilic and reactive functional groups, enhances phase separation and leads to increased porosity[38]. However, this also results in fragility of the scaffold's microstructure, which may compromise mechanical integrity. The macro-image (Figure 2D″) further highlights this, showing an irregular, highly porous surface. Although the increased Ch content improves hydrophilicity and surface area, which are favorable for cell attachment and nutrient diffusion, careful optimization is necessary to ensure mechanical stability for specific tissue engineering application.

Quantitative image analysis was subsequently performed to complement the qualitative SEM observations. For each scaffold formulation, three independent fields of view (n = 3 per sample, magnification ×100) were analyzed using ImageJ to determine surface porosity and apparent pore size distribution, and the results are summarized in Table 2. Pure PGSu exhibited a porosity of 53.1 ± 5.2 % with a mean pore diameter of 27.7 ± 56.4 µm, consistent with its relatively dense microstructure. PGSu/Ch (70/30) displayed a porosity of 51.1 ± 4.9 % and a mean pore diameter of 40.9 ± 68.7 µm, indicating slightly larger but fewer pores compared with PGSu. PGSu/Ch (30/70) exhibited the largest mean pore diameter (66.6 ± 102.5 µm) and highest porosity (72.3 ± 6.4 %), reflecting a highly open and interconnected network. PGSu/Ch (50/50) showed a porosity of 71.5 ± 6.1 % but smaller mean pores (24.0 ± 49.2 µm), suggesting a dense but highly interconnected architecture.

These quantitative results establish a clear composition-dependent relationship between chitosan content and scaffold microstructure. The denser PGSu and PGSu/Ch (70/30) structures may provide better initial mechanical support, whereas the highly porous PGSu/Ch (30/70) and PGSu/Ch (50/50) scaffolds are expected to promote faster cell infiltration and nutrient transport. This tunable structure–property relationship enables the rational selection of scaffold composition for applications requiring either higher mechanical integrity or accelerated tissue integration.

Table 2. Quantitative analysis of surface porosity and average pore size for PGSu and PGSu/Ch scaffolds based on ImageJ segmentation of SEM micrographs

Sample	Average Pore Size (µm)	Porosity (%)
PGSu	27.7 ± 56.4	53.1 ± 5.2
PGSu70/Ch30	40.9 ± 68.7	51.1 ± 4.9
PGSu30/Ch70	66.6 ± 102.5	72.3 ± 6.4
PGSu50/Ch50	24.0 ± 49.2	71.5 ± 6.1

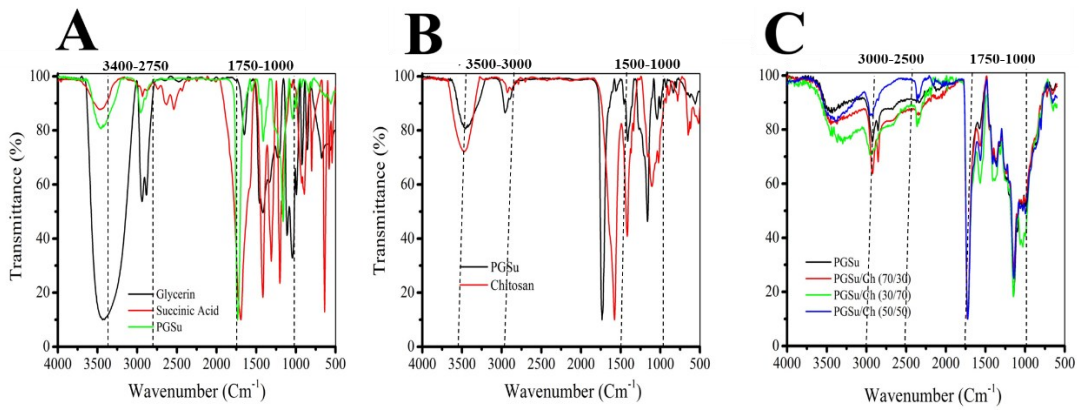

Figure 1. (A) FTIR spectra of glycerin, succinic acid, and PGSu. (B) FTIR spectra of PGSu and chitosan (Ch). (C) FTIR spectra of PGSu/Ch scaffolds with different weight ratios (70/30, 30/70, 50/50)

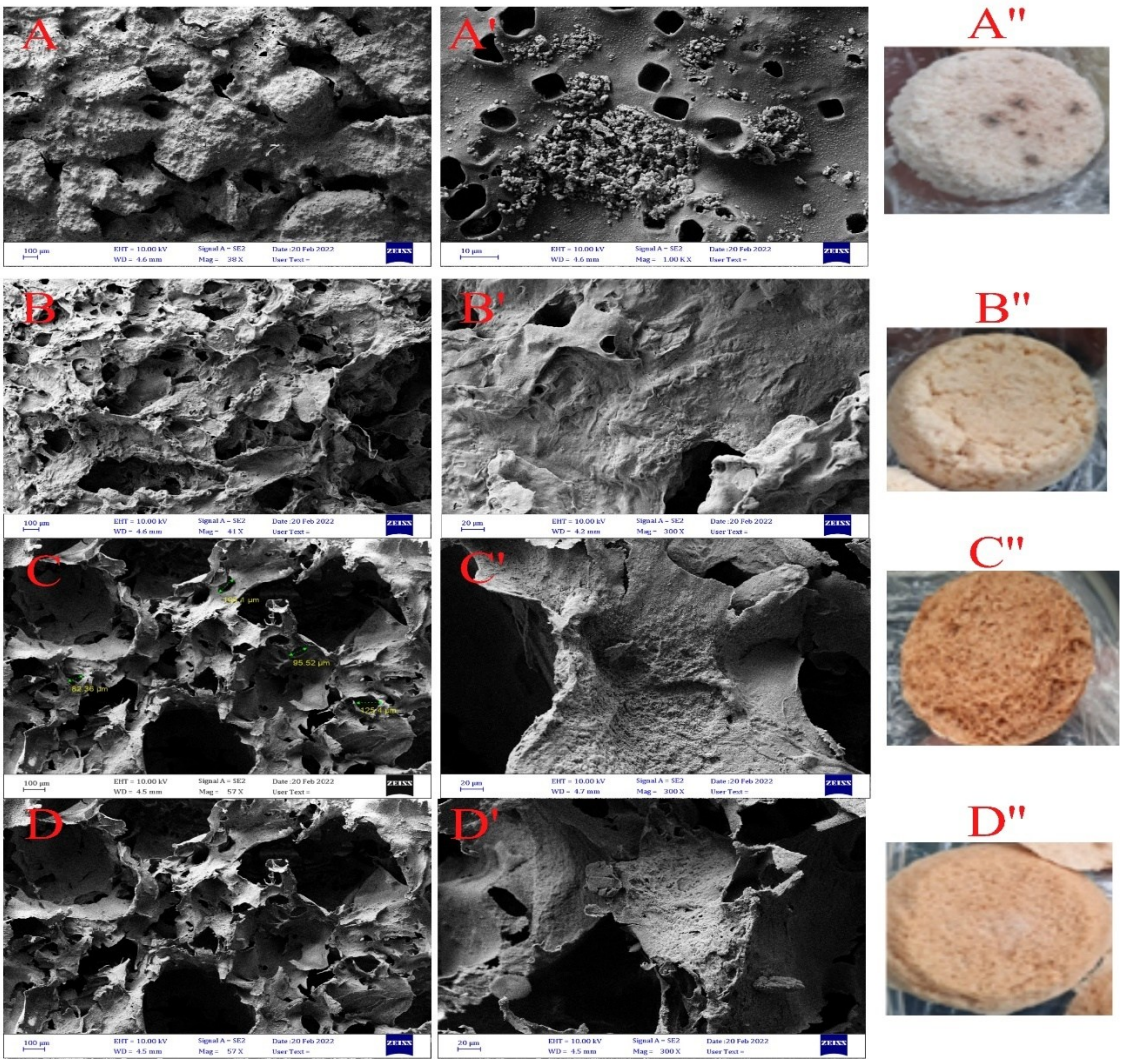

Figure 2. SEM micrographs of studied samples at two magnifications with scale bars included (100 µm for left panels and 20 µm for right panels), along with photographs of the actual scaffolds. (A, A', A") PGSu, (B, B', B") PGSu/Ch (70/30), (C, C', C") PGSu/Ch (3/70), and (D, D', D") PGSu/Ch (50/50)

Although SEM micrographs revealed a smooth and continuous surface morphology, no tribological or coefficient-of-friction tests were performed in this study. The low surface roughness observed qualitatively suggests that the scaffolds may exhibit reduced friction when interfacing with surrounding soft tissues, which could minimize local shear stresses and irritation. However, a comprehensive tribological characterization, including coefficient of friction and wear analysis under physiologically relevant conditions, is recommended for future studies to validate this hypothesis. The relatively smooth surface and interconnected porosity of the scaffolds can be attributed to the selection of PGSu as the base polyester, the hydrogen-bonding interactions

introduced by chitosan, and the controlled salt-leaching process with fine NaCl particles. These design choices likely contributed to reduced surface roughness and lower interfacial drag, which are beneficial for minimizing local shear stress at the tissue–scaffold interface. Nonetheless, direct tribological characterization is necessary in future work to quantitatively confirm this effect.

Despite the observed improvements in surface smoothness, several limiting factors prevent the scaffold from achieving a truly frictionless interface. The hydrophilic nature of chitosan leads to swelling, which may induce micro-roughness over time. Minor heterogeneity in crosslink density and pore-wall irregularities inherent to the salt-leaching process can also contribute to local variations in surface energy. Furthermore, in vivo conditions introduce adsorbed proteins and extracellular matrix components that modify surface interactions and may increase friction relative to the pristine material. These factors suggest that while friction is reduced compared to unmodified systems, complete elimination is not feasible, and a certain level of interface resistance remains beneficial for mechanical stability and integration.

3.3. XRD, TGA, and Mechanical Analysis

The crystalline structure of the fabricated scaffolds was analyzed using XRD, and the corresponding results are shown in Figure 3A. Pure PGSu displayed a broad diffraction peak centered at approximately 2Θ= 20.44°, indicative of its predominantly amorphous nature. This is consistent with the typical structure of aliphatic polyesters synthesized via polycondensation[39]. Upon incorporation of Ch, a progressive increase in peak intensity was observed across the PGSu/Ch composites, with the PGSu/Ch (50/50) sample exhibiting the most pronounced peak. This suggests enhanced molecular ordering and semi-crystalline behavior. The increase in crystallinity may be attributed to hydrogen bonding between hydroxyl and amine groups in Ch and ester linkages in PGSu, promoting regular chain alignment and reducing system entropy[40]. To further interpret the structural arrangement, the interplanar spacing (d-spacing) was estimated using Bragg's law Equation (2)[41], based on the observed peak at 2θ = 20.44°, assuming first-order diffraction and a Cu Kα radiation wavelength of 1.5406 Å. The resulting spacing was calculated to be approximately 4.34 Å. This relatively compact interplanar distance implies closer molecular packing within the semi-crystalline domains of the scaffold[42].

$$n\lambda = 2\sin\Theta \quad (2)$$

Also, the enhanced crystallinity in the PGSu/Ch (50/50) sample may also contribute to its improved compressive strength by facilitating tighter chain packing and increased structural rigidity[43]. To provide a semi-quantitative measure of ordering consistent with the XRD profiles, an apparent crystallinity index (CI_app) was estimated by deconvoluting the crystalline contribution from the amorphous halo and integrating areas according to Equation (3):

$$CI_{app} = \frac{A_c}{A_c + A} \quad (3)$$

where A_c and A_a are the integrated areas of the crystalline and amorphous components, respectively. Using a uniform baseline and Voigt peak fitting on the plotted patterns, CI_{app} increased from 22.4% (PGSu) to 29.6% [PGSu/Ch (70/30)], 33.1% [PGSu/Ch (30/70)], and 38.7% [PGSu/Ch (50/50)]. These values corroborate the visual increase in peak prominence at 20.4°, confirming that Ch incorporation enhances molecular ordering beyond mere peak height changes.

The thermal stability of the scaffolds was evaluated using TGA, as shown in Figure 3B. All samples exhibited a major weight loss between 250 °C and 400 °C, corresponding to the thermal degradation of polymer backbones. The degradation curves exhibited two distinguishable thermal events. The initial weight loss between 250–320 °C is attributed to the cleavage of side chains and lower molecular weight oligomers[44], while the second major phase (350–450 °C) corresponds to the scission of the primary ester backbone[45]. These multi-stage profiles reflect the heterogeneous architecture and compositional complexity of the scaffolds[46]. Moreover, the distinct degradation steps suggest the presence of phase-separated domains with differing thermal responses, likely resulting from partial miscibility of PGSu and Ch at the molecular level[47]. Pure PGSu displayed the lowest thermal stability, with an earlier onset of degradation and the lowest residual mass at 600 °C, suggesting a faster decomposition rate. This observation may be attributed to the low crosslinking density and absence of thermal stabilizing interactions in the pure PGSu matrix, which allows greater chain mobility and earlier thermal scission under increasing temperature [48][49].

Upon incorporation of Ch, the thermal degradation profile changed notably. The PGSu/Ch (30/70) scaffold demonstrated the highest thermal resistance, characterized by a delayed onset of degradation and the greatest residual mass at 600 °C. This improvement is likely due to stronger hydrogen bonding between PGSu and Ch and the inherent thermal insulating nature of Ch, which collectively hinder chain mobility and delay

decomposition [50]. The PGSu/Ch (50/50) and (70/30) scaffolds also showed improved thermal stability compared to pure PGSu, although to a lesser extent than the (30/70) blend. These results indicate that increasing Ch content enhances thermal resistance up to an optimal ratio, beyond which excessive chitosan may reduce the uniformity of the matrix, slightly lowering thermal performance. Overall, the PGSu/Ch (30/70) formulation exhibited the most favorable thermal behavior for biomedical applications requiring improved thermal endurance.

The mechanical properties of the scaffolds were evaluated under both dry and wet conditions, as presented in Figures 3C and 3D. Under dry conditions (Figure 3C), pure PGSu exhibited the highest elongation at break (40%), reflecting its elastomeric nature and high chain mobility[10]; however, it showed the lowest compressive strength (300 Pa), highlighting its mechanical weakness under load-bearing conditions. Incorporation of Ch into the PGSu matrix led to a significant enhancement in compressive strength, accompanied by a reduction in elongation. Notably, the PGSu/Ch (50/50) scaffold exhibited the highest compressive modulus (1500 Pa), indicating improved load-bearing capacity. This enhancement is likely attributed to stronger interpolymer hydrogen bonding and increased structural density[51]. The improved crystallinity observed in this composition (Figure 3A) may also contribute to its superior mechanical performance. In contrast, the PGSu/Ch (70/30) sample showed a moderate increase in stiffness but maintained higher elasticity than the 50/50 blend, suggesting partial reinforcement without excessive rigidity. Under hydrated conditions (Figure 3D), all samples demonstrated reduced compressive strength due to water-induced plasticization. Despite this, the PGSu/Ch (50/50) scaffold retained the highest compressive strength (1000 Pa), suggesting its structural integrity remains largely preserved even in wet environments. Interestingly, the PGSu/Ch (30/70) scaffold showed the highest elongation at break (45%) in the wet state, indicating enhanced flexibility and water-responsive swelling behavior. This behavior can be attributed to the high hydrophilicity of Ch, which increases water uptake and reduces matrix cohesion. While this composition sacrifices some mechanical strength, its increased ductility may be advantageous for applications requiring flexibility and conformability. This viscoelastic, hydrated behavior mimics the mechanical profile of native ECM, particularly in dynamic tissues such as dermis and peripheral nerves[52]. Scaffolds exhibiting such compliance can reduce mechanical mismatch with host tissue, minimize fibrosis, and improve integration and regeneration outcomes[53]. This enhancement likely stems from synergistic interactions at the molecular level, including interfacial hydrogen bonding and physical entanglements between PGSu and Ch[54]. These interactions improve energy dissipation under stress and distribute load more uniformly across the polymer matrix, minimizing localized failure[55]. The cylindrical disk-shaped scaffolds produced by the salt-leaching process (Scheme 1) were specifically designed for unconfined compression testing, which is the most physiologically relevant loading mode for dermal, subcutaneous, and peripheral nerve applications. Under *in vivo* conditions, such scaffolds primarily experience multidirectional compressive and viscoelastic forces generated by interstitial fluid pressure, swelling, and surrounding tissue contraction, rather than uniaxial tension. Highly porous scaffolds are also prone to premature failure when subjected to tensile gripping, which may lead to artifactual results and poor reproducibility. Therefore, compression testing under both dry and hydrated states was prioritized in this study to capture clinically relevant mechanical compliance and ensure meaningful comparison between scaffold compositions.

In summary, the mechanical performance of the scaffolds is highly dependent on Ch content. The 50/50 formulation provides an optimal balance between stiffness and elasticity, making it suitable for soft tissue engineering applications that require both mechanical support and durability. In contrast, the 30/70 composition, with its higher flexibility and swelling potential, may be better suited for tissues that experience dynamic deformation or require conformal interface integration, such as skin or peripheral nerve regeneration.

3.4. Contact angles and Swelling analysis

The wettability of the fabricated scaffolds was assessed by dynamic contact angle measurements, and the results are presented in Figure 4A. Water droplets were deposited on the scaffold surfaces, and images were recorded at 0, 15, and 30 seconds. The contact angle of pure PGSu remained relatively high throughout the measurement period, indicating its low hydrophilicity. This limited wettability is attributed to the esterification of hydroxyl and carboxyl groups during polymerization, which reduces the number of available polar functional groups at the surface[56].

In contrast, the incorporation of Ch significantly increased the hydrophilicity of the scaffolds[57]. Among the composite formulations, PGSu/Ch (30/70) exhibited the lowest contact angle at 30 seconds, reflecting superior water affinity. This behavior can be attributed to the abundance of hydrophilic functional groups (–OH

and –NH_2) in Ch, as well as potential hydrogen bonding interactions at the surface. In addition, the orientation and surface exposure of these polar groups during scaffold formation may further enhance surface energy, lowering the contact angle and facilitating rapid wetting kinetics, particularly in the PGSu/Ch (30/70) formulation.[58] The higher Ch content also facilitates greater surface roughness and porosity, as confirmed by SEM images, further enhancing water absorption dynamics.

Swelling behavior of the scaffolds was analyzed over a 50-hour period, and the results are shown in Figure 4B. All samples exhibited time-dependent water uptake, with PGSu/Ch (30/70) demonstrating the highest swelling ratio, reaching nearly 75% after 50 hours. This significant water uptake can be correlated with the porous microstructure and high free volume resulting from chitosan's hygroscopic nature, which enables capillary-driven absorption and retention of aqueous media within the scaffold matrix[59]. The enhanced swelling in this formulation can be linked to its high Ch content, which increases hydrophilicity, free volume, and the ability to absorb and retain water[60]. The PGSu/Ch (50/50) and PGSu/Ch (70/30) samples showed intermediate swelling behaviors, while pure PGSu exhibited the lowest swelling capacity.

The observed trends in both wettability and swelling support the notion that increasing Ch content improves water interaction characteristics of the scaffold. These properties are critical for tissue engineering applications, as they promote better nutrient transport, facilitate cellular infiltration, and enhance the overall bioactivity of the scaffold matrix. Moreover, enhanced swelling and wettability can create a hydrated, ECM-like microenvironment that facilitates protein adsorption, promotes initial cell adhesion, and supports early-stage tissue integration — all of which are essential for effective scaffold–host interaction *in vivo*[61].

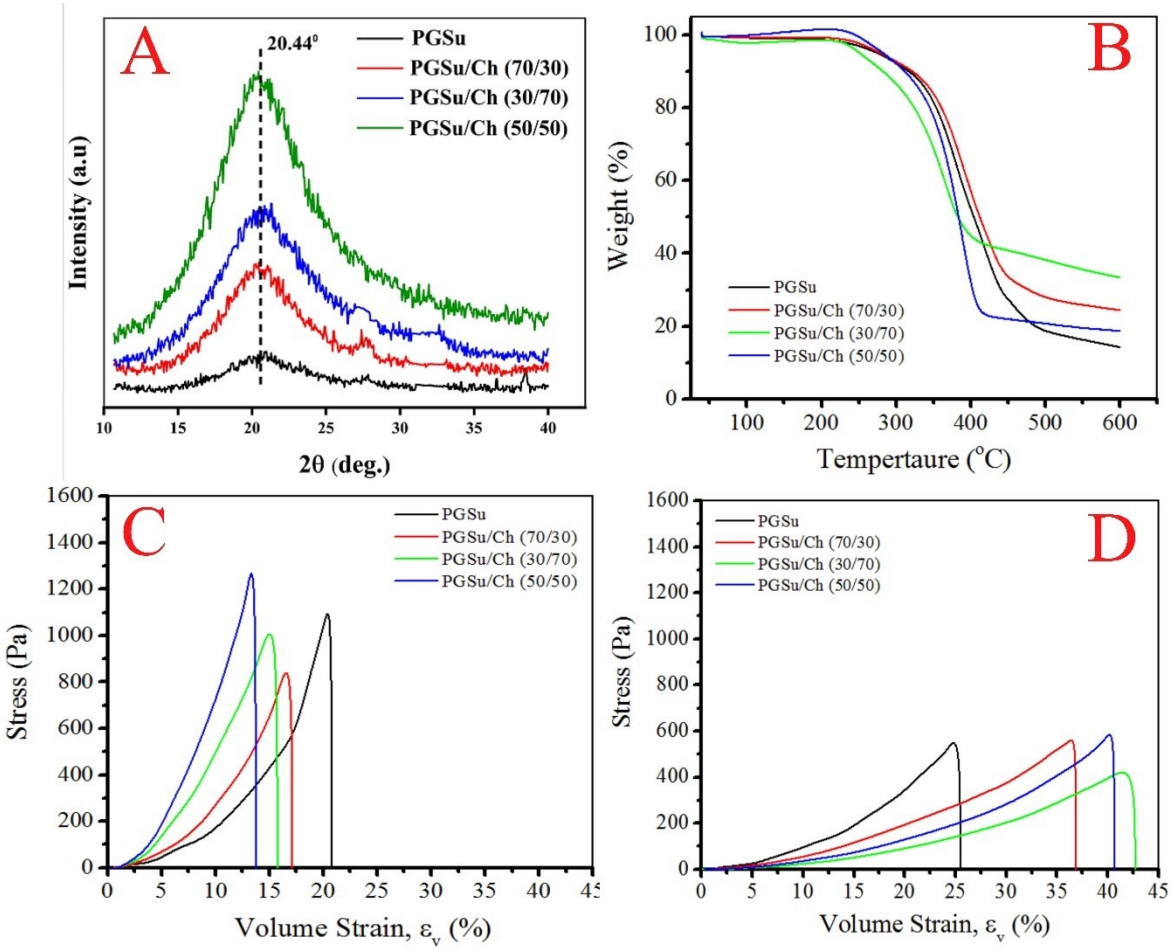

Figure 3. (A) XRD analysis, (B) TGA analysis, compressive mechanical analysis of studied samples in (C) dry condition and (D) wet condition

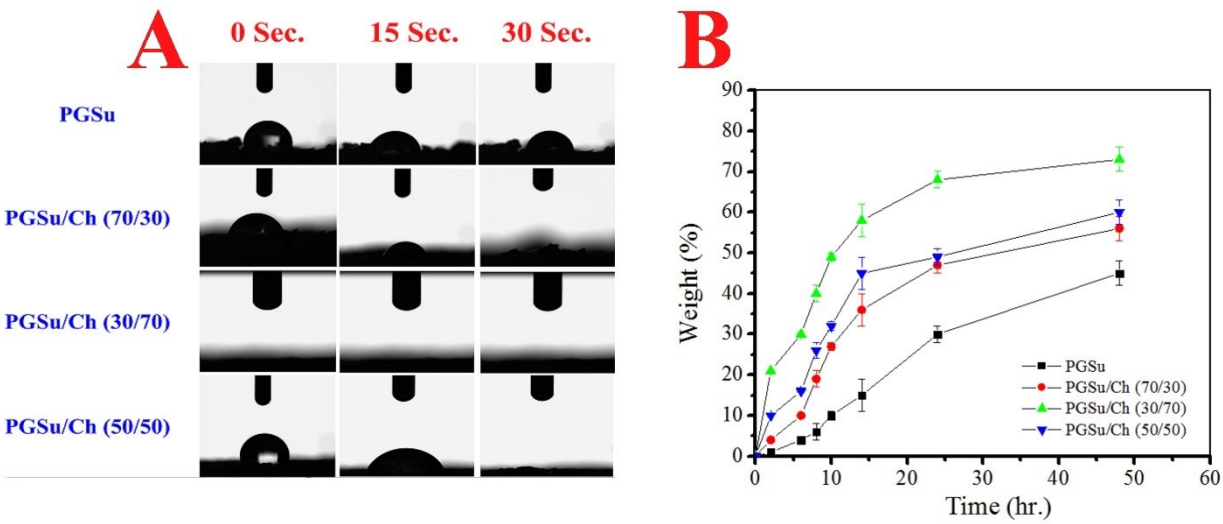

Figure 4. (A) Contact angle measurements of PGSu and PGSu/Ch scaffolds with different weight ratios (70/30, 30/70, 50/50) recorded at 0, 15, and 30 seconds. (B) Swelling behavior of PGSu and PGSu/Ch scaffolds with different weight ratios as a function of time

3.5. Correlation between Mechanical Properties and hydrolytic Degradation

The hydrolytic degradation behavior of the scaffolds was evaluated in fetal bovine serum (FBS) over a period of 60 days, and the results are presented in Figure 5A. Pure PGSu exhibited the lowest weight loss throughout the degradation period, with only 31.2 ± 2.1% mass loss at day 20, 45.8 ± 2.4% at day 30, and 92.4 ± 3.1% after 60 days of incubation. This slower degradation can be attributed to its dense crosslinked structure and limited hydrophilic functionality, which restrict water penetration into the polymer network [62]. The dense network acts as a physical barrier against aqueous penetration, while the low density of polar groups limits water-mediated ester hydrolysis, thereby maintaining structural integrity over extended periods [63]. Incorporation of Ch significantly increased the degradation rate, with PGSu/Ch (30/70) showing the highest mass loss (15.2 ± 1.5% at day 20, 25.5 ± 1.8% at day 30, and 65.2 ± 1.9% at day 60), followed by PGSu/Ch (50/50) (20.1 ± 1.7%, 32.4 ± 2.0%, 78.5 ± 2.3%) and PGSu/Ch (70/30) (26.5 ± 1.9%, 40.6 ± 2.3%, 86.8 ± 2.7%), with all pairwise differences being statistically significant. This behavior is likely due to the higher content of hydrophilic groups (–OH and –NH_2) in Ch, which facilitate water uptake and hydrolysis of ester bonds [64]. Additionally, the presence of proton-donating and -accepting groups in Ch can catalyze localized acid–base reactions that accelerate chain scission, particularly at hydrated microdomains [65]. Overall, the degradation rate followed the trend: PGSu < PGSu/Ch (70/30) < PGSu/Ch (50/50) < PGSu/Ch (30/70). These results underline the importance of compositional tuning for achieving optimal mechanical integrity. The observed cohesion and compressive strength of the PGSu/Ch scaffolds result from the synergistic effects of polymer composition, intermolecular hydrogen bonding, optimized crosslink density, and uniformly interconnected porosity. The 50/50 formulation exhibited the best mechanical performance due to an optimal balance of flexibility and network density. Future improvements may be achieved by further optimizing crosslinking chemistry, incorporating nanoscale reinforcements for enhanced load-bearing capacity, and employing gradient porosity or bioreactor-based preconditioning to promote extracellular matrix deposition before implantation.

To assess the mechanical implications of degradation, compression tests were performed after 20 and 30 days of incubation in FBS, and the results are shown in Figure 5B and 5C, respectively. A significant reduction in compressive strength and strain was observed across all samples, reflecting the progressive breakdown of the internal network structure. The decline in mechanical performance was more pronounced in samples with higher Ch content, particularly PGSu/Ch (30/70), consistent with its higher degradation rate. This mechanical softening can be directly attributed to the disruption of load-bearing microstructures and loss of cohesive crosslinks, which undermines the scaffold's capacity to resist compressive deformation under physiological loads[66].

Further insights into structural deterioration were obtained via SEM imaging of the scaffold surfaces after 20 and 30 days of degradation (Figures 5D–F). The initial three-dimensional porous architecture observed before degradation became progressively disrupted. After 20 days (Figures 5D–E), microcracks and thinning of pore walls were evident. By day 30 (Figure 5F), substantial collapse of the pore structure and loss of

interconnectivity were observed, confirming advanced degradation. The evolution from a well-interconnected to a fragmented porous structure, as visualized via SEM, supports the hypothesis of hydrolytic weakening at the pore walls, leading to progressive microstructural collapse and compromised tissue integration potential. A schematic illustration (Figures 5G) summarizes the degradation process, showing how the scaffold's internal structure becomes increasingly disorganized as crosslinked networks break down, leading to changes in pore geometry and loss of mechanical integrity.

These results highlight a clear correlation between scaffold composition, hydrolytic stability, and mechanical performance over time. While higher Ch content enhances hydrophilicity and degradation rate—beneficial for bioresorption—it also accelerates mechanical deterioration. Therefore, tailoring the PGSu/Ch ratio allows modulation of degradation kinetics to match the intended application and tissue regeneration timeline.

The superior compressive performance observed for PGSu/Ch (50/50) can be attributed to an optimal balance between network density and hydrophilicity. At this composition, sufficient chitosan is present to enhance intermolecular hydrogen bonding, thereby improving load transfer and viscoelastic response, without introducing excessive hydrophilicity that could over-plasticize the polymer network. In contrast, the faster degradation of PGSu/Ch (30/70) results from its higher density of hydrophilic –OH and –NH_2 groups, which enhance water uptake, disrupt crosslink density, and promote hydrolytic chain scission. The greater pore interconnectivity of this composition likely facilitates fluid penetration, accelerating ester bond cleavage and mechanical softening.

When compared with benchmark soft tissue engineering scaffolds, our PGSu/Ch (50/50) scaffolds demonstrate a hydrated compressive modulus of 180 kPa, which is slightly higher than that reported by Liu et al. [67] for PGS-based scaffolds (167.0 kPa) and comparable to the range of 170–200 kPa reported by Wang et al. [68] for PGS@Gel scaffolds. Unlike PLA- or PCL-based scaffolds, which are significantly stiffer and degrade over several months to years, PGSu/Ch composites offer faster yet controlled degradation (65–92% mass loss over 60 days) that better matches the timeline of soft tissue regeneration. Furthermore, the presence of chitosan provides intrinsic bioactivity and cell-interactive functionality not present in purely synthetic polyesters, positioning PGSu/Ch scaffolds as promising candidates for next-generation soft tissue engineering platforms requiring a balance of mechanical compliance, tunable degradation, and biological performance.

3.6. In vitro analysis

The biocompatibility of the fabricated scaffolds was assessed by MTT assay, and the results are presented in Figure 6. Cell viability was measured after 1, 4, and 7 days of incubation. On day 1, all scaffolds exhibited comparable levels of cell viability, indicating initial cytocompatibility and absence of acute cytotoxicity. This suggests that none of the materials released harmful byproducts during early cell contact. By day 4, a noticeable increase in cell viability was observed across all samples, particularly in the PGSu/Ch (30/70) and PGSu/Ch (70/30) scaffolds. The increased hydrophilicity and favorable surface properties, as previously confirmed by contact angle and swelling analyses, likely contributed to enhanced cell adhesion and proliferation. On day 7, the PGSu/Ch (30/70) scaffold demonstrated the highest cell viability, even exceeding the control group, indicating not only excellent cytocompatibility but also bioactivity that promotes cell proliferation. The high Ch content in this formulation provides abundant amino and hydroxyl groups that improve surface interactions and potentially stimulate cellular metabolic activity[69]. The PGSu/Ch (50/50) scaffold also supported sustained viability, though slightly lower than S3. The pure PGSu scaffold exhibited consistently high cell viability across all time points, comparable to the control group. This suggests that despite lacking bioactive additives such as Ch, PGSu itself is cytocompatible and does not induce acute or long-term cytotoxicity. However, samples containing Ch, particularly PGSu/Ch (30/70), demonstrated even higher cell viability on day 7, indicating enhanced bioactivity due to the presence of amine- and hydroxyl-rich functional groups that promote cell proliferation.

These results confirm that the incorporation of Ch into PGSu scaffolds significantly enhances cytocompatibility and supports time-dependent cell proliferation, with PGSu/Ch (30/70) emerging as the most favorable formulation for promoting *in vitro* cell growth.

To evaluate early-stage cell–material interactions, cell adhesion on the scaffold surfaces was investigated after 1 day of culture using SEM. Representative micrographs at low, medium, and high magnifications are shown in Figure 7 for each sample group.

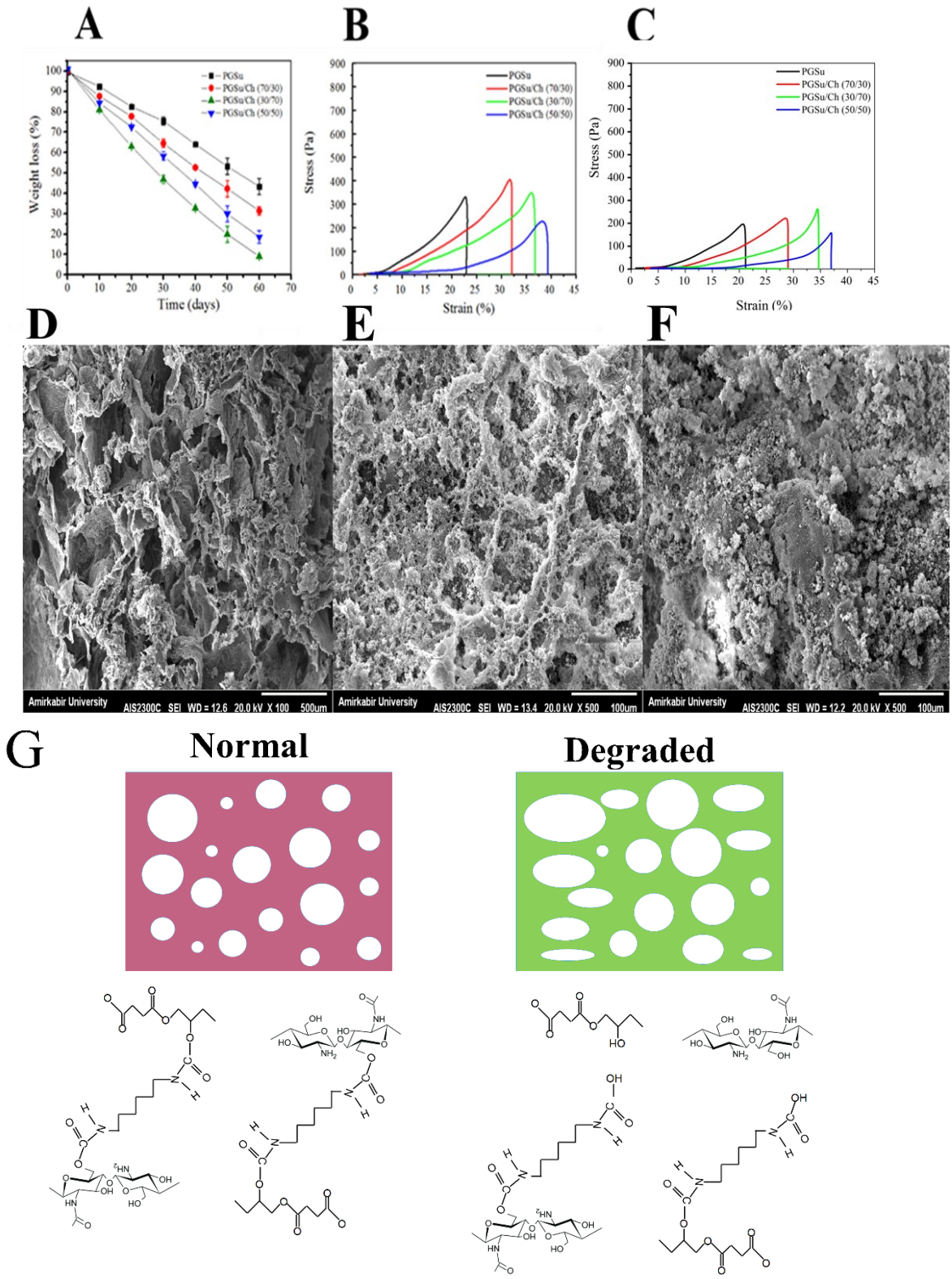

Figure 5. (A) Hydrolytic degradation profiles of PGSu and PGSu/Ch composite scaffolds over 60 days in FBS. (B, C) Compressive mechanical behavior of scaffolds after 20 and 30 days of degradation, respectively. (D–F) SEM micrographs showing surface morphological changes after 20 and 30 days of degradation with scale bars (500 µm for D and 100 µm for E, F). (G) Schematic illustration of the degradation process and corresponding chemical bond cleavage within the scaffold matrix

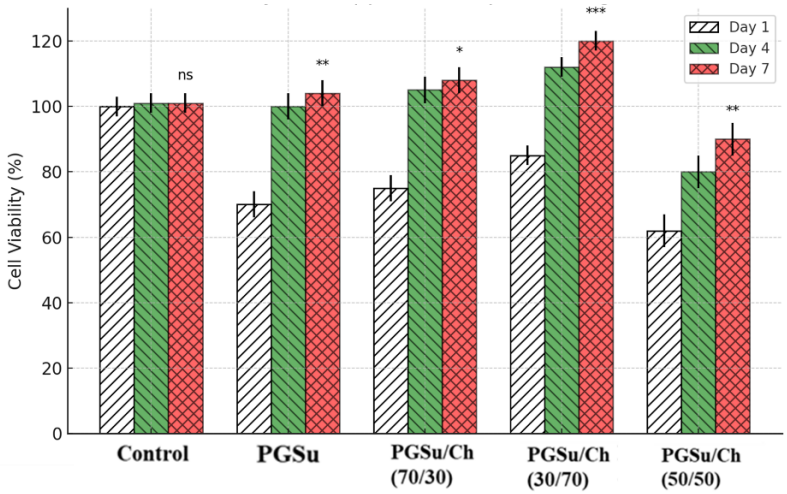

Figure 6. Cell viability of L929 fibroblasts cultured on PGSu and PGSu/Ch composite scaffolds over 1, 4, and 7 days, as assessed by MTT assay. Results are presented as mean ± SD (n = 3). A significant increase in cell viability was observed over time, particularly for PGSu/Ch (30/70) and PGSu/Ch (50/50) scaffolds, indicating excellent cytocompatibility and support for cell proliferation. Statistical analysis was performed using one-way ANOVA followed by Tukey's post hoc test. Significance levels are indicated as ns (not significant), $p < 0.05$ (*), $p < 0.01$ (**), and $p < 0.001$ (***)

The pure PGSu scaffold (Figure 7A–A″) displayed a relatively smooth surface with limited cell attachment. The absence of abundant surface functional groups and lower hydrophilicity likely restricted effective cell anchorage. In contrast, all PGSu/Ch composite scaffolds demonstrated enhanced cell adhesion, indicating that the incorporation of Ch significantly improved scaffold bioactivity. Among the composite samples, PGSu/Ch (30/70) and PGSu/Ch (50/50) scaffolds (Figures 7C–C″ and 7D–D″) showed a notably higher density of adhered cells. The cells appeared well spread with visible pseudopodia extensions, suggesting active interaction with the underlying matrix. This improvement can be attributed to the synergistic effects of Ch's hydrophilic and bioactive functional groups (–OH, –NH_2), which facilitate protein adsorption and integrin-mediated cell binding[70]. The porous and rough surface morphology, as observed in previous SEM results, further enhances cellular contact area and attachment potential. The PGSu/Ch (70/30) scaffold (Figures 7B–B″) exhibited moderate cell adhesion, with fewer attached cells compared to higher Ch-content samples, yet significantly more than pure PGSu. These observations confirm that increasing Ch content improves the scaffold's cell-adhesive properties at the early stages, likely due to the combined effects of enhanced surface chemistry and wettability.

Collectively, these results demonstrate that PGSu/Ch scaffolds, particularly at 50/50 and 30/70 ratios, provide a favorable surface for initial cell attachment, which is critical for subsequent cell proliferation and tissue integration.

To assesses longer-term cell–scaffold interactions, the adhesion of cells to the scaffold surfaces was analyzed after 4 days of culture using SEM imaging at multiple magnifications, as shown in Figure 8.

The pure PGSu scaffold (Figures 8A–A″) displayed minimal cell presence, with only a few loosely attached, rounded cells observed. The lack of cell spreading and interaction with the surface suggests poor compatibility, consistent with the low hydrophilicity and limited bioactive functional groups of PGSu[71]. In comparison, the PGSu/Ch (70/30) scaffold (Figures 8B–B″) demonstrated improved cell adhesion. The scaffold surface showed several cells with early signs of spreading and partial integration into the matrix. This moderate improvement is likely due to the partial presence of Ch, which enhances surface hydrophilicity and provides bioactive sites for attachment. Notably, PGSu/Ch (30/70) (Figures 8C–C″) and PGSu/Ch (50/50) (Figures 8D–D″) scaffolds exhibited superior cell adhesion behavior. In these samples, the scaffold surfaces were heavily colonized by numerous well-spread cells, many displaying flattened morphologies and pseudopodia-like extensions indicative of active cellular interaction. The presence of Ch in higher ratios promotes favorable surface chemistry, including hydroxyl and amine groups, which improve protein adsorption and integrin-mediated binding[72][73]. Additionally, the rough and porous topography further facilitates cellular anchorage and expansion. Between these two, the PGSu/Ch (50/50) scaffold showed the highest cell density and more developed cell clusters, suggesting stronger scaffold–cell interaction and more efficient support of cellular activity. These observations align well with previous MTT assay results, which also indicated high viability for this composition.

Overall, these findings reinforce the role of Ch in

enhancing early and sustained cell adhesion, with PGSu/Ch (50/50) and PGSu/Ch (30/70) demonstrating the most favorable cell–material interactions by day 4.

Cell adhesion and proliferation on the scaffolds were further examined after 7 days of culture using SEM imaging, with results shown in Figure 9. This long-term observation provides insights into scaffold performance in supporting sustained cell–material interactions.

In the case of pure PGSu (Figures 9A–A″), although a slight increase in the number of adhered cells compared to earlier time points was observed, the overall cell coverage remained limited. Most cells appeared rounded with minimal spreading, indicating weak adhesion and insufficient surface bioactivity to support robust colonization [74]. The PGSu/Ch (70/30) scaffold (Figures 9B–B″) exhibited an improved cellular response. Cells were more numerous and slightly more spread, suggesting better interactions with the matrix, yet the level of surface colonization remained moderate. In contrast, the PGSu/Ch (30/70) (Figures 9C–C″) and PGSu/Ch (50/50) (Figures 9D–D″) scaffolds demonstrated excellent cell adhesion and coverage. In both samples, cells formed dense clusters and extensive spreading was evident, with visible cytoplasmic extensions anchoring into the scaffold surface. The porous and hydrophilic environment provided by higher Ch content likely facilitates cellular infiltration and nutrient exchange, promoting enhanced proliferation and adhesion. Notably, the PGSu/Ch (30/70) scaffold showed the highest cell density and surface integration. The architecture supported not only adhesion but also apparent colony formation, indicating favorable conditions for long-term cell survival and potential tissue ingrowth.

These results align well with MTT assay trends and earlier adhesion assessments, confirming that higher Ch incorporation enhances scaffold bioactivity over extended periods.

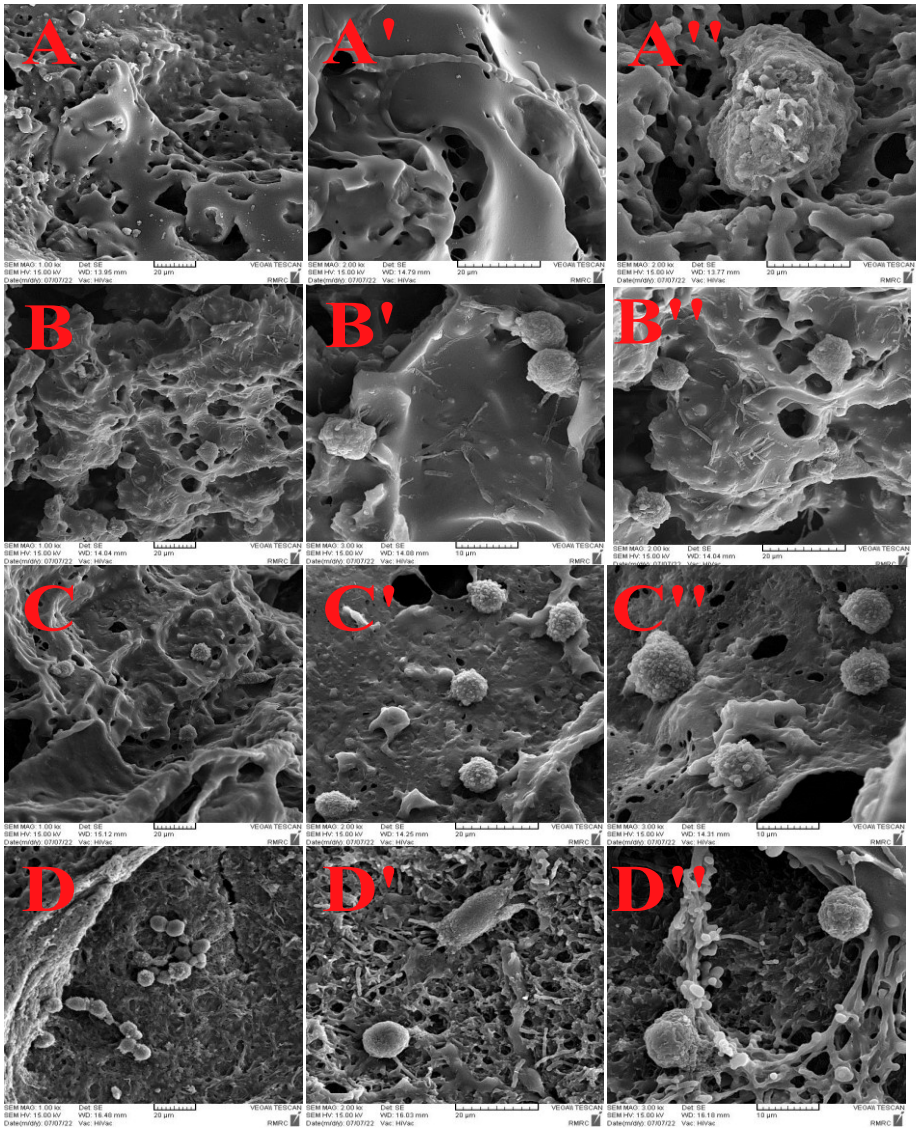

Figure 7. SEM micrographs showing cell adhesion on the scaffold surfaces after 1 day of culture at increasing magnifications (scale bars: 20 µm for left and middle columns, 10 µm for right column). (A–A″) PGSu, (B–B″) PGSu/Ch (70/30), (C–C″) PGSu/Ch (30/70), and (D–D″) PGSu/Ch (50/50)

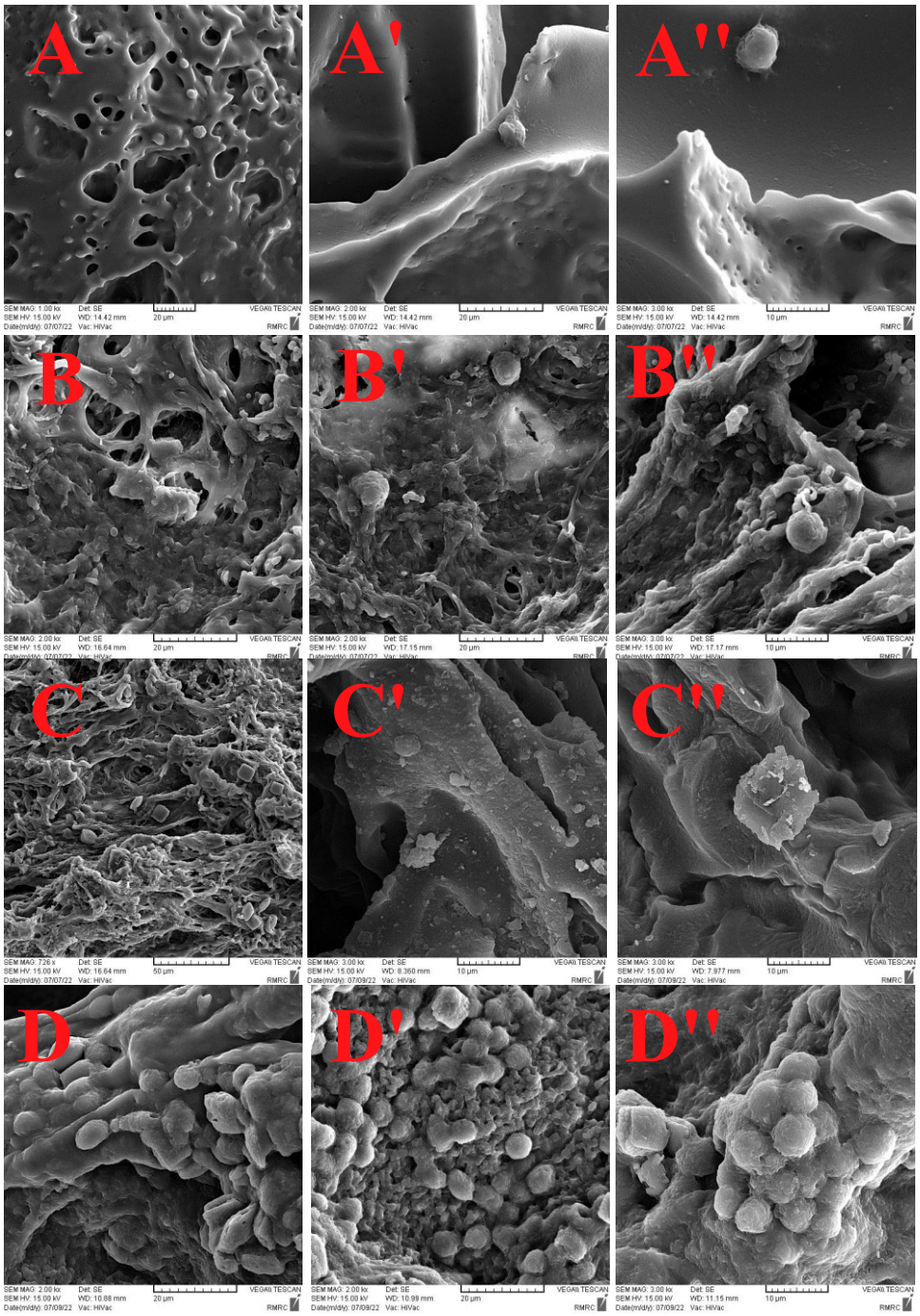

Figure 8. SEM micrographs showing cell adhesion on scaffold surfaces after 4 days of culture at increasing magnifications (scale bars: 20 µm for left and middle columns, 10 µm for right column). (A–A″) PGSu, (B–B″) PGSu/Ch (70/30), (C–C″) PGSu/Ch (30/70), and (D–D″) PGSu/Ch (50/50)

In the preceding sections, we have systematically presented the structural, mechanical, degradation, and biological data of PGSu/Ch scaffolds and compared them with those reported in the literature to position our findings in the broader scientific context. Previous investigations, such as those by Zabihi et al. [11] (PGSu nanogels), Mahtabi et al. [15] (PLA/PGSu/nHA bone scaffolds), and Zhang et al. [19] (PGS–silk fibroin–Ch composites), have highlighted the promise of glycerol-based polyesters and chitosan for regenerative medicine but exhibited notable limitations. These included an absence of three-dimensional porous scaffold systems, lack of systematic optimization across multiple weight ratios, limited mechanical testing under physiologically relevant hydrated conditions, and insufficient quantitative correlation between scaffold composition, crystallinity, porosity, mechanical properties, and cellular performance.

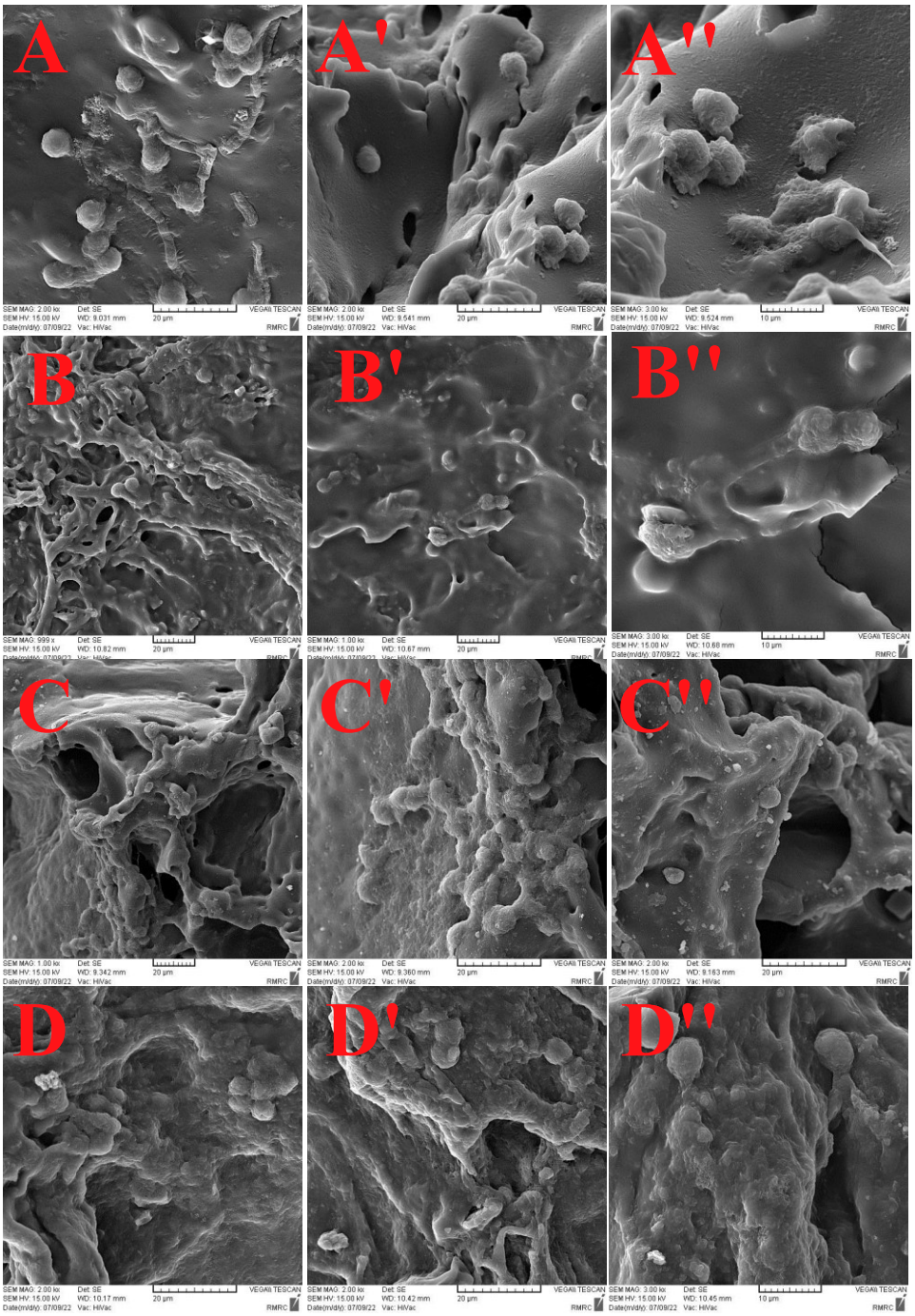

Figure 9. SEM micrographs showing cell adhesion on scaffold surfaces after 7 days of culture at increasing magnifications (scale bars: 20 µm for left and middle columns, 10 µm for right column). (A–A″) PGSu, (B–B″) PGSu/Ch (70/30), (C–C″) PGSu/Ch (30/70), and (D–D″) PGSu/Ch (50/50)

The present study addresses these gaps by implementing a multi-ratio design (70/30, 50/50, 30/70), quantitative CI_{app} analysis (e.g., 38.7% for PGSu/Ch 50/50), and compression testing under both dry and hydrated states, yielding a hydrated compressive modulus of ≈180 kPa—higher than typical values reported for pure PGS scaffolds (167 kPa)—and establishing a direct link between chain ordering and mechanical performance. The degradation profile was also characterized in detail, with PGSu/Ch (30/70) exhibiting 65–92 % mass loss over 60 days, a rate that better matches soft tissue remodeling than the months-to-years degradation of PLA or PCL scaffolds. Furthermore, in vitro assays confirmed superior fibroblast viability and attachment, quantitatively validating and extending the qualitative trends reported in earlier chitosan-containing composites.

Collectively, these results demonstrate that PGSu/Ch scaffolds can be tuned to simultaneously provide interconnected macroporosity, mechanical compliance, and controlled resorption, thereby minimizing mechanical mismatch and reducing risks of fibrosis or

chronic inflammation. By integrating structure–property–function relationships, this work provides a reproducible and translationally relevant framework for rational scaffold design in skin, subcutaneous, and peripheral nerve repair.

Despite these advances, certain limitations remain. Our work was restricted to in vitro assessments with fibroblasts, and no *in vivo* studies were conducted to evaluate immune response, vascularization, or long-term functional recovery. Additionally, while salt-leaching is a robust and scalable method, advanced fabrication techniques such as 3D printing or gradient-porosity approaches could further optimize scaffold architecture for site-specific applications. Future research should therefore focus on (i) *in vivo* validation in relevant animal models, (ii) integration of growth factors or bioactive nanoparticles to enhance regenerative signaling, and (iii) computational modeling or AI-assisted design to tailor scaffold performance to patient-specific requirements.

4. Conclusions

In this study, a series of bioengineered three-dimensional porous scaffolds were successfully fabricated by combining PGSu with varying weight ratios of Ch using a salt-leaching approach. Comprehensive characterization confirmed the successful synthesis and integration of components: FTIR verified the formation of PGSu and its chemical interaction with Ch, while XRD revealed increased molecular ordering in Ch-containing scaffolds, particularly in the PGSu/Ch (50/50) formulation. SEM analysis demonstrated that increasing Ch content produced a more open and interconnected porous architecture, favoring water penetration and cellular infiltration. Wettability and swelling studies further confirmed enhanced hydrophilicity for Ch-containing scaffolds, with PGSu/Ch (30/70) showing the highest water uptake. TGA results indicated improved thermal stability with higher Ch content, supporting the structural integrity of the scaffolds during processing and sterilization. Mechanical testing revealed that PGSu/Ch (50/50) possessed the highest compressive strength and modulus (180 kPa in hydrated state), a result attributable to an optimal network density and enhanced hydrogen bonding that provide efficient load transfer without compromising elasticity. In contrast, PGSu/Ch (30/70) displayed the greatest elongation at break and mechanical compliance, suggesting its suitability for dynamic tissue environments requiring flexible scaffolds. Hydrolytic degradation studies demonstrated a composition-dependent trend, with PGSu/Ch (30/70) showing the fastest mass loss (65% over 60 days), which correlates with its higher hydrophilicity and greater pore interconnectivity that accelerate hydrolytic chain scission. *In vitro* cytocompatibility assessment through MTT assay and SEM-based cell adhesion studies confirmed excellent biocompatibility for all formulations, with PGSu/Ch (30/70) supporting the highest cell viability, robust attachment, and active proliferation over 7 days. This highlights the dual potential of PGSu/Ch scaffolds: PGSu/Ch (50/50) is ideal for applications requiring longer structural support during tissue regeneration (e.g., subcutaneous tissue or vascular grafts), while PGSu/Ch (30/70) is suited for situations where rapid integration and resorption are desirable, such as wound healing, dermal repair, and peripheral nerve regeneration.

These findings underscore the versatility of PGSu/Ch composites as next-generation biomaterials offering tunable mechanical compliance, controllable biodegradation, and excellent cytocompatibility for personalized soft tissue engineering. Nevertheless, this study has certain limitations. The current work was confined to in vitro analysis, and *in vivo* studies are essential to evaluate tissue response, vascularization potential, and long-term integration. Furthermore, while residual solvents and crosslinkers were minimized by prolonged washing, sensitive analytical methods should be employed in future work to ensure complete removal and confirm biosafety for clinical use.

Future directions will include tensile, cyclic loading, creep, and stress relaxation tests to fully capture the viscoelastic behavior, hysteresis, and fatigue tolerance of the scaffolds under conditions mimicking repeated physiological loading. These measurements will provide critical insights into long-term durability, energy dissipation, and resistance to mechanical failure, complementing the static compression results presented in this study. Furthermore, *in vivo* implantation studies will be performed to evaluate immune response, angiogenesis, and tissue integration, and bioreactor-based dynamic culture systems will be employed to better simulate physiological microenvironments and pre-condition scaffolds before implantation. Additional strategies such as surface functionalization through covalent grafting will be explored, taking advantage of the abundant hydroxyl and amine groups in PGSu/Ch to immobilize bioactive peptides (e.g., RGD sequences), growth factors, or anti-inflammatory agents using chemistries such as EDC/NHS coupling or click reactions. Such grafting approaches are expected to enhance cell adhesion, direct lineage-specific differentiation, and improve tissue–scaffold integration. Furthermore, PEGylation or zwitterionic grafting could be employed to modulate protein adsorption and reduce inflammatory responses, while grafting of mechanically

reinforcing moieties could increase interfacial cohesion and wear resistance. Finally, incorporation of bioactive nanoparticles, gradient-porosity design, and advanced fabrication techniques such as 3D printing will be investigated to synergistically enhance angiogenesis, extracellular matrix deposition, and site-specific regenerative outcomes.

Funding
None

Authors Contribution
All authors have contributed equally to prepare the paper.

Availability of data and materials
The datasets used and/or analysed during the current study available from the corresponding author on reasonable request.

Conflict of interests
The authors declare that they have no known competing financial interests or personal relationships that could have appeared to influence the work reported in this paper.

Reference

[1]. F. Hosseini Chenani, V. F. Rezaei, V. Fakhri, F. R. Wurm, L. Uzun, and V. Goodarzi, "Green synthesis and characterization of poly(glycerol-azelaic acid) and its nanocomposites for applications in regenerative medicine," J. Appl. Polym. Sci., vol. 138, no. 24, p. 50563, Jun. 2021. doi: https://doi.org/10.1002/APP.50563;WGROUP:STRING:PUBLICATION

[2]. S. M. Shabestari *et al.*, "Role of phosphate-modified cellulose into the scaffold based on poly (glycerol azelaic acid)-co-poly(ε-caprolactone) for using bone regenerative medicine," *Int. J. Biol. Macromol.*, vol. 304, p. 140855, Apr. 2025. doi: https://doi.org/10.1016/j.ijbiomac.2025.140855

[3]. N. Kasoju and A. Sunilkumar, "Convergence of tissue engineering and sustainable development goals," *Biotechnol. Sustain. Mater.*, vol. 1, no. 1, p. 20, Dec. 2024. doi: https://doi.org/10.1186/s44316-024-00021-y

[4]. M. Pourmadadi *et al.*, "Development of Poly(ether sulfone)/Poly(vinyl alcohol)/Magnesium-Doped Carbon Quantum Dot Scaffolds for Bone Tissue Engineering," *ACS Biomater. Sci. Eng.*, Apr. 2025. doi: https://doi.org/10.1021/ACSBIOMATERIALS.4C02124

[5]. H. Vilaça-Faria, J. Noro, R. L. Reis, and R. P. Pirraco, "Extracellular matrix-derived materials for tissue engineering and regenerative medicine: A journey from isolation to characterization and application," *Bioact. Mater.*, vol. 34, pp. 494–519, Apr. 2024. doi: https://doi.org/10.1016/j.bioactmat.2024.01.004

[6]. Z. Chen *et al.*, "Progress in biomaterials inspired by the extracellular matrix," *Giant*, vol. 19, p. 100323, Aug. 2024. doi: https://doi.org/10.1016/j.giant.2024.100323

[7]. T. Urbánek, E. Jäger, A. Jäger, and M. Hrubý, "Selectively Biodegradable Polyesters: Nature-Inspired Construction Materials for Future Biomedical Applications," *Polymers (Basel).*, vol. 11, no. 6, p. 1061, Jun. 2019. doi: https://doi.org/10.3390/polym11061061

[8]. L. Vogt, F. Ruther, S. Salehi, and A. R. Boccaccini, "Poly(Glycerol Sebacate) in Biomedical Applications—A Review of the Recent Literature," *Adv. Healthc. Mater.*, vol. 10, no. 9, May 2021. doi: https://doi.org/10.1002/adhm.202002026

[9]. M. Jiang *et al.*, "Progress of succinic acid production from renewable resources: Metabolic and fermentative strategies," *Bioresource Technology*, vol. 245, no. Pt B. Bioresour Technol, pp. 1710–1717, Dec. 01, 2017. doi: https://doi.org/10.1016/j.biortech.2017.05.209

[10]. S. Seyfikar, M. Asgharnejad-laskoukalayeh, S. H. Jafari, V. Goodarzi, M. H. Salehi, and S. Zamanlui, "Introducing a new approach to preparing bionanocomposite sponges based on poly(glycerol sebacate urethane) (PGSU) with great interconnectivity and high hydrophilicity properties for application in tissue engineering," *Eur. Polym. J.*, vol. 173, p. 111239, Jun. 2022. doi: https://doi.org/10.1016/j.eurpolymj.2022.111239

[11]. F. Zabihi, H. Koeppe, K. Achazi, S. Hedtrich, and R. Haag, "One-Pot Synthesis of Poly(glycerol- co-succinic acid) Nanogels for Dermal Delivery," *Biomacromolecules*, vol. 20, no. 5, pp. 1867–1875, May 2019. doi: https://doi.org/10.1021/acs.biomac.8b01741

[12]. N. R. Luman, K. A. Smeds, and M. W. Grinstaff, "The Convergent Synthesis of Poly(glycerol-succinic acid) Dendritic Macromolecules," *Chem. - A Eur. J.*, vol. 9, no. 22, pp. 5618–5626, Nov. 2003 doi: https://doi.org/10.1002/chem.200305172

[13]. B. Tan, S. Bi, K. Emery, and M. J. Sobkowicz, "Bio-based poly(butylene succinate-co-hexamethylene succinate) copolyesters with tunable thermal and mechanical properties," *Eur. Polym. J.*, vol. 86, pp. 162–172, Jan. 2017. doi: https://doi.org/10.1016/j.eurpolymj.2016.11.017

[14]. A. L. Sisson, D. Ekinci, and A. Lendlein, "The contemporary role of ε-caprolactone chemistry to create advanced polymer architectures," *Polymer*, vol. 54, no. 17. Elsevier, pp. 4333–4350, Aug. 02, 2013. doi: https://doi.org/10.1016/j.polymer.2013.04.045

[15]. R. Mahtabi, S. Z. Benisi, V. Goodarzi, and S. Shojaei, "Application of Biodegradable Bone Scaffolds Based on Poly(Lactic Acid) / Poly(Glycerol Succinic Acid) Containing Nano-Hydroxyapatite," *J. Polym. Environ.*, vol. 32, no. 2, pp. 548–559, Feb. 2024. doi: https://doi.org/10.1007/s10924-023-02983-y

[16]. V. Fakhri, M. Monem, G. Mir Mohamad Sadeghi, H. A. Khonakdar, V. Goodarzi, and N. Karimpour-Motlagh, "Impact of poly(ε-caprolactone) on the thermal, dynamicmechanical and crystallization behavior of polyvinylidene fluoride/poly(ε-caprolactone) blends in the presence of KIT-6 mesoporous particles," Polym. Adv. Technol., vol. 32, no. 11, pp. 4424–4439, Nov. 2021. doi: https://doi.org/10.1002/PAT.5444;JOURNAL:JOURNAL:10991581;WGROUP:STRING:PUBLICATIO N

[17]. V. Taghipour-Sabzevar et al., "Targeted delivery of a short

antimicrobial peptide against CD44-overexpressing tumor cells using hyaluronic acid-coated chitosan nanoparticles: An in vitro study," J. Nanoparticle Res., vol. 22, no. 5, pp. 1–16, May 2020. doi: https://doi.org/10.1007/S11051-020-04838-2/METRICS

[18]. X. Dong *et al.*, "A chitosan based scaffold with enhanced mechanical and biocompatible performance for biomedical applications," *Polym. Degrad. Stab.*, vol. 181, p. 109322, Nov. 2020. doi: https://doi.org/10.1016/J.POLYMDEGRADSTAB.2020.109322

[19]. X. Zhang, C. Jia, X. Qiao, T. Liu, and K. Sun, "Silk fibroin microfibers and chitosan modified poly (glycerol sebacate) composite scaffolds for skin tissue engineering," *Polym. Test.*, vol. 62, pp. 88–95, Sep. 2017. doi: https://doi.org/10.1016/j.polymertesting.2017.06.012

[20]. M. Asgharnejad-laskoukalayeh *et al.*, "Preparation and characterization of a new sustainable bio-based elastomer nanocomposites containing poly(glycerol sebacate citrate)/chitosan/n-hydroxyapatite for promising tissue engineering applications," *J. Biomater. Sci. Polym. Ed.*, vol. 33, no. 18, pp. 2385–2405, 2022. doi: https://doi.org/10.1080/09205063.2022.2104600

[21]. S. Saravani, M. Ebrahimian-Hosseinabadi, and D. Mohebbi-Kalhori, "Polyglycerol sebacate/chitosan/gelatin nano-composite scaffolds for engineering neural construct," *Mater. Chem. Phys.*, vol. 222, pp. 147–151, Jan. 2019. doi: https://doi.org/10.1016/j.matchemphys.2018.10.010

[22]. M. Rostamian *et al.*, "Introducing a bio sorbent for removal of methylene blue dye based on flexible poly(glycerol sebacate)/chitosan/graphene oxide ecofriendly nanocomposites," *Chemosphere*, vol. 289, Feb. 2022. doi: https://doi.org/10.1016/j.chemosphere.2021.133219

[23]. V. Fakhri, C. H. Su, M. Tavakoli Dare, M. Bazmi, A. Jafari, and V. Pirouzfar, "Harnessing the power of polyol-based polyesters for biomedical innovations: synthesis, properties, and biodegradation," *Journal of Materials Chemistry B*, vol. 11, no. 40. The Royal Society of Chemistry, pp. 9597–9629, Oct. 18, 2023. doi: https://doi.org/10.1039/d3tb01186k

[24]. W. Wang, C. Xue, and X. Mao, "Chitosan: Structural modification, biological activity and application," *International Journal of Biological Macromolecules*, vol. 164. Elsevier, pp. 4532–4546, Dec. 01, 2020. doi: https://doi.org/10.1016/j.ijbiomac.2020.09.042

[25]. S. Lu *et al.*, "A Cellulose/Chitosan Dual Cross-Linked Multifunctional and Resilient Hydrogel for Emergent Open Wound Management," *Adv. Healthc. Mater.*, vol. 13, no. 13, p. 2304676, May 2024. doi: https://doi.org/10.1002/adhm.202304676

[26]. M. Selim, H. M. Mousa, G. T. Abdel-Jaber, A. Barhoum, and A. Abdal-hay, "Innovative designs of 3D scaffolds for bone tissue regeneration: Understanding principles and addressing challenges," *European Polymer Journal*, vol. 215. Pergamon, p. 113251, Jul. 17, 2024. doi: https://doi.org/10.1016/j.eurpolymj.2024.113251

[27]. K. Shukla, A. Arunagiri, and K. Muthukumar, "Synthesis and hydrolytic degradation of poly (glycerol succinate) based polyesters," *J. Indian Chem. Soc.*, vol. 100, no. 1, p. 100841, Jan. 2023. doi: https://doi.org/10.1016/j.jics.2022.100841

[28]. M. Agach, S. Marinkovic, B. Estrine, and V. Nardello-Rataj, "Acyl Poly(Glycerol-Succinic Acid) Oligoesters: Synthesis, Physicochemical and Functional Properties, and Biodegradability," *J. Surfactants Deterg.*, vol. 19, no. 5, pp. 933–941, Sep. 2016. doi: https://doi.org/10.1007/s11743-016-1853-4

[29]. B. Godinho, R. Nogueira, N. Gama, and A. Ferreira, "Synthesis and Characterization of Poly(glycerol sebacate), Poly(glycerol succinate) and Poly(glycerol sebacate-co-succinate)," *J. Polym. Environ.*, vol. 32, no. 9, pp. 4330–4347, Sep. 2024. doi: https://doi.org/10.1007/S10924-024-03212-W/FIGURES/11

[30]. M. Agach, S. Delbaere, S. Marinkovic, B. Estrine, and V. Nardello-Rataj, "Characterization, stability and ecotoxic properties of readily biodegradable branched oligoesters based on bio-sourced succinic acid and glycerol," in *Polymer Degradation and Stability*, Elsevier, Oct. 2012, pp. 1956–1963. doi: https://doi.org/10.1016/j.polymdegradstab.2012.03.026

[31]. G. S. Foo, J. J. Lee, C. H. Chen, S. E. Hayes, C. Sievers, and C. W. Jones, "Elucidation of Surface Species through in Situ FTIR Spectroscopy of Carbon Dioxide Adsorption on Amine-Grafted SBA-15," *ChemSusChem*, vol. 10, no. 1, pp. 266–276, Jan. 2017. doi: https://doi.org/10.1002/cssc.201600809

[32]. I. Silvestro *et al.*, "Preparation and characterization of TPP-chitosan crosslinked scaffolds for tissue engineering," *Materials (Basel).*, vol. 13, no. 16, p. 3577, Aug. 2020. doi: https://doi.org/10.3390/MA13163577

[33]. B. Pidhatika *et al.*, "Advancing Bone Regeneration: The Impactful Role of Plasma Technology," *Plasma Processes and Polymers*, vol. 22, no. 2. John Wiley & Sons, Ltd, p. 2400171, Feb. 01, 2024. doi: https://doi.org/10.1002/ppap.202400171

[34]. A. Henke, S. Kadlubowski, P. Ulanski, J. M. Rosiak, and K. F. Arndt, "Radiation-induced cross-linking of polyvinylpyrrolidone-poly(acrylic acid) complexes," in *Nuclear Instruments and Methods in Physics Research, Section B: Beam Interactions with Materials and Atoms*, North-Holland, Jul. 2005, pp. 391–398. doi: https://doi.org/10.1016/j.nimb.2005.04.003

[35]. B. Kost *et al.*, "The influence of the functional end groups on the properties of polylactide-based materials," *Progress in Polymer Science*, vol. 130. 2022. doi: https://doi.org/10.1016/j.progpolymsci.2022.101556

[36]. L. K. Njaramba, Y. Yoon, and C. M. Park, "Fabrication of porous beta-cyclodextrin functionalized PVDF/Fe–MOF mixed matrix membrane for enhanced ciprofloxacin removal," *npj Clean Water*, vol. 7, no. 1, pp. 1–13, Mar. 2024. doi: https://doi.org/10.1038/s41545-024-00312-x

[37]. Y. Mino, N. Fukukawa, and H. Matsuyama, "Simulation on Pore Formation from Polymer Solution at Surface in Contact with Solid Substrate via Thermally Induced Phase Separation," *Membranes (Basel).*, vol. 11, no. 7, p. 527, Jul. 2021.

doi: https://doi.org/10.3390/membranes11070527

[38]. S. B. Rekik, S. Gassara, J. Bouaziz, A. Deratani, and S. Baklouti, "Enhancing hydrophilicity and permeation flux of chitosan/kaolin composite membranes by using polyethylene glycol as porogen," *Appl. Clay Sci.*, vol. 168, pp. 312–323, Feb. 2019.
doi: https://doi.org/10.1016/j.clay.2018.11.029

[39]. S. Farjaminejad, S. Shojaei, V. Goodarzi, H. Ali Khonakdar, and M. Abdouss, "Tuning properties of bio-rubbers and its nanocomposites with addition of succinic acid and ε-caprolactone monomers to poly(glycerol sebacic acid) as main platform for application in tissue engineering," *Eur. Polym. J.*, vol. 159, p. 110711, Oct. 2021.
doi: https://doi.org/10.1016/j.eurpolymj.2021.110711

[40]. M. Chen *et al.*, "Hydrogen bonding impact on chitosan plasticization," *Carbohydr. Polym.*, vol. 200, pp. 115–121, Nov. 2018.
doi: https://doi.org/10.1016/j.carbpol.2018.07.062

[41]. M. Pourmadadi *et al.*, "Green Synthesis of pH-Sensitive Carboxymethyl Cellulose/Agarose/Carbon Quantum Dots Nanocarriers for Quercetin Delivery to A549 Lung Cancer Using an Emulsification Method," *Bionanoscience*, vol. 14, no. 4, pp. 4570–4584, Nov. 2024.
doi: https://doi.org/10.1007/s12668-024-01426-9

[42]. R. A. Pascal, C. M. Wang, G. C. Wang, and L. V. Koplitz, "Ideal molecular conformation versus crystal site symmetry," *Cryst. Growth Des.*, vol. 12, no. 9, pp. 4367–4376, Sep. 2012.
doi: https://doi.org/10.1021/cg300374w

[43]. K. Pathak *et al.*, "Biomedical Applications of Quaternized Chitosan," *Polymers (Basel).*, vol. 13, no. 15, p. 2514, Jul. 2021.
doi: https://doi.org/10.3390/polym13152514

[44]. B. Kost *et al.*, "The influence of the functional end groups on the properties of polylactide-based materials," *Progress in Polymer Science*, vol. 130. Pergamon, p. 101556, Jul. 01, 2022.
doi: https://doi.org/10.1016/j.progpolymsci.2022.101556

[45]. N. M. Nurazzi *et al.*, "Thermogravimetric analysis properties of cellulosic natural fiber polymer composites: A review on influence of chemical treatments," *Polymers (Basel).*, vol. 13, no. 16, 2021.
doi: https://doi.org/10.3390/polym13162710

[46]. W. Guo *et al.*, "3D printing of multifunctional gradient bone scaffolds with programmable component distribution and hierarchical pore structure," *Compos. Part A Appl. Sci. Manuf.*, vol. 166, p. 107361, Mar. 2023.
doi: https://doi.org/10.1016/j.compositesa.2022.107361

[47]. A. M. Torres-Huerta, D. Palma-Ramírez, M. A. Domínguez-Crespo, D. Del Angel-López, and D. De La Fuente, "Comparative assessment of miscibility and degradability on PET/PLA and PET/chitosan blends," *Eur. Polym. J.*, vol. 61, pp. 285–299, Dec. 2014.
doi: https://doi.org/10.1016/j.eurpolymj.2014.10.016

[48]. K. Chrissafis, K. M. Paraskevopoulos, and D. N. Bikiaris, "Thermal degradation mechanism of poly(ethylene succinate) and poly(butylene succinate): Comparative study," *Thermochim. Acta*, vol. 435, no. 2, pp. 142–150, Sep. 2005.
doi: https://doi.org/10.1016/j.tca.2005.05.011

[49]. G. S. A. Suleiman, X. Zeng, R. Chakma, I. Y. Wakai, and Y. Feng, "Recent advances and challenges in thermal stability of PVA-based film: A review," *Polymers for Advanced Technologies*, vol. 35, no. 2. John Wiley & Sons, Ltd, p. e6327, Feb. 01, 2024.
doi: https://doi.org/10.1002/pat.6327

[50]. I. Younes and M. Rinaudo, "Chitin and Chitosan Preparation from Marine Sources. Structure, Properties and Applications," *Mar. Drugs*, vol. 13, no. 3, pp. 1133–1174, Mar. 2015.
doi: https://doi.org/10.3390/md13031133

[51]. L. E. Makar, N. Nady, A. Abd El-Fattah, N. Shawky, and S. H. Kandil, "Unmodified Gum Arabic/Chitosan/Nanohydroxyapatite Nanocomposite Hydrogels as Potential Scaffolds for Bone Regeneration," *Polymers (Basel).*, vol. 14, no. 15, p. 3052, Jul. 2022.
doi: https://doi.org/10.3390/polym14153052

[52]. J. Nicolas, S. Magli, L. Rabbachin, S. Sampaolesi, F. Nicotra, and L. Russo, "3D Extracellular Matrix Mimics: Fundamental Concepts and Role of Materials Chemistry to Influence Stem Cell Fate," *Biomacromolecules*, vol. 21, no. 6, pp. 1968–1994, 2020.
doi: https://doi.org/10.1021/acs.biomac.0c00045

[53]. D. Huang *et al.*, "Viscoelasticity in natural tissues and engineered scaffolds for tissue reconstruction," *Acta Biomaterialia*, vol. 97. Elsevier, pp. 74–92, Oct. 01, 2019.
doi: https://doi.org/10.1016/j.actbio.2019.08.013

[54]. M. R. Tuttle, S. T. Davis, and S. Zhang, "Synergistic Effect of Hydrogen Bonding and π-πStacking Enables Long Cycle Life in Organic Electrode Materials," *ACS Energy Lett.*, vol. 6, no. 2, pp. 643–649, Feb. 2021.
doi: https://doi.org/10.1021/acsenergylett.0c02604

[55]. A. M. Feizi and F. Taheri-Behrooz, "Fatigue life prediction of polymer matrix composites containing initial delamination using thermography," *Polym. Test.*, vol. 145, p. 108751, Apr. 2025.
doi: https://doi.org/10.1016/J.POLYMERTESTING.2025.108751

[56]. M. Drobota, S. Ursache, and M. Aflori, "Surface Functionalities of Polymers for Biomaterial Applications," *Polymers (Basel).*, vol. 14, no. 12, p. 2307, Jun. 2022.
doi: https://doi.org/10.3390/polym14122307

[57]. A. Haider *et al.*, "Chitosan as a tool for tissue engineering and rehabilitation: Recent developments and future perspectives – A review," *Int. J. Biol. Macromol.*, vol. 278, p. 134172, Oct. 2024.
doi: https://doi.org/10.1016/j.ijbiomac.2024.134172

[58]. M. Kalin and M. Polajnar, "The correlation between the surface energy, the contact angle and the spreading parameter, and their relevance for the wetting behaviour of DLC with lubricating oils," *Tribol. Int.*, vol. 66, pp. 225–233, Oct. 2013.
doi: https://doi.org/10.1016/j.triboint.2013.05.007

[59]. M. N. Alam and L. P. Christopher, "Natural Cellulose-Chitosan Cross-Linked Superabsorbent Hydrogels with Superior Swelling Properties," *ACS Sustain. Chem. Eng.*, vol. 6, no. 7, pp. 8736–8742, Jul. 2018.
doi: https://doi.org/10.1021/acssuschemeng.8b01062

[60]. M. Saberian, R. Safari Roudsari, N. Haghshenas, A. Rousta, and S. Alizadeh, "How the combination of alginate and chitosan can fabricate a hydrogel with favorable properties for wound healing," *Heliyon*, vol. 10, no. 11, p. e32040, Jun. 2024. doi: https://doi.org/10.1016/j.heliyon.2024.e32040

[61]. S. Guo *et al.*, "Parallel Control over Surface Charge and Wettability Using Polyelectrolyte Architecture: Effect on Protein Adsorption and Cell Adhesion," *ACS Appl. Mater. Interfaces*, vol. 8, no. 44, pp. 30552–30563, Nov. 2016. doi: https://doi.org/10.1021/acsami.6b09481

[62]. H. Mndlovu, P. Kumar, L. C. du Toit, and Y. E. Choonara, "A review of biomaterial degradation assessment approaches employed in the biomedical field," *npj Mater. Degrad.*, vol. 8, no. 1, p. 66, Jul. 2024. doi: https://doi.org/10.1038/s41529-024-00487-1

[63]. L. Solhi *et al.*, "Understanding Nanocellulose-Water Interactions: Turning a Detriment into an Asset," *Chem. Rev.*, vol. 123, no. 5, pp. 1925–2015, 2023. doi: https://doi.org/10.1021/acs.chemrev.2c00611

[64]. L. Yu *et al.*, "Exploring the potent hydrolytic activity of chitosan-cerium complex microspheres resin for organophosphorus pesticide degradation," *Heliyon*, vol. 10, no. 13, p. e33642, Jul. 2024. doi: https://doi.org/10.1016/j.heliyon.2024.e33642

[65]. R. Ahorsu, M. Constanti, and F. Medina, "Recent Impacts of Heterogeneous Catalysis in Biorefineries," *Ind. Eng. Chem. Res.*, vol. 60, no. 51, pp. 18612–18626, 2021. doi: https://doi.org/10.1021/acs.iecr.1c02789

[66]. W. Cai *et al.*, "Biomechanics in bone regeneration and mechanobiology in osteoblasts: Fundamental concepts and recent progress," *EngMedicine*, vol. 2, no. 1, p. 100057, Mar. 2025. doi: https://doi.org/10.1016/J.ENGMED.2025.100057

[67]. Y. Y. Liu, C. Intini, M. Dobricic, F. J. O'Brien, J. LLorca, and M. Echeverry-Rendon, "Collagen-based 3D printed poly (glycerol sebacate) composite scaffold with biomimicking mechanical properties for enhanced cartilage defect repair," *Int. J. Biol. Macromol.*, vol. 280, p. 135827, Nov. 2024. doi: https://doi.org/10.1016/J.IJBIOMAC.2024.135827

[68]. S. Wang *et al.*, "Gelatin-modified 3D printed PGS elastic hierarchical porous scaffold for cartilage regeneration," *APL Bioeng.*, vol. 7, no. 3, pp. 1–12, 2023. doi: https://doi.org/10.1063/5.0152151

[69]. Z. Liu, K. Wang, X. Peng, and L. Zhang, "Chitosan-based drug delivery systems: Current strategic design and potential application in human hard tissue repair," *European Polymer Journal*, vol. 166. Pergamon, p. 110979, Mar. 05, 2022. doi: https://doi.org/10.1016/j.eurpolymj.2021.110979

[70]. Y. Zhu, Y. Zhang, and Y. Zhou, "Application Progress of Modified Chitosan and Its Composite Biomaterials for Bone Tissue Engineering," *Int. J. Mol. Sci.*, vol. 23, no. 12, 2022. doi: https://doi.org/10.3390/ijms23126574

[71]. I. Junkar, "Interaction of cells and platelets with biomaterial surfaces treated with gaseous plasma," in *Advances in Biomembranes and Lipid Self-Assembly*, vol. 23, Academic Press, 2016, pp. 25–59. doi: https://doi.org/10.1016/bs.abl.2016.01.002

[72]. M. Ul-Islam, K. F. Alabbosh, S. Manan, S. Khan, F. Ahmad, and M. W. Ullah, "Chitosan-based nanostructured biomaterials: Synthesis, properties, and biomedical applications," *Adv. Ind. Eng. Polym. Res.*, vol. 7, no. 1, pp. 79–99, Jan. 2024. doi: https://doi.org/10.1016/j.aiepr.2023.07.002

[73]. S. M. Shabestari *et al.*, "pH-responsive chitosan-sodium alginate nanocarriers for curcumin delivery against brain cancer," *Colloids Surfaces B Biointerfaces*, vol. 255, no. March, 2025. doi: https://doi.org/10.1016/j.colsurfb.2025.114875

[74]. M. Afshari, M. Pourmadadi, S. M. Shabestari, H. Abdouss, and M. Abdouss, "Development and Characterization of biocompatible Gelatin/Polyethylene Glycol/Copper-Doped carbon quantum Dots@Curcumin nanocarriers for pH-Sensitive curcumin delivery in glioblastoma treatment," *Inorg. Chem. Commun.*, vol. 179, no. P2, p. 114782, Sep. 2025. doi: https://doi.org/10.1016/j.inoche.2025.114782